Applied Mathematical Modelling 56 (2018) 626–647

Contents lists available at ScienceDirect

Applied Mathematical Modelling

journal homepage: www.elsevier.com/locate/apm

Topology optimization considering the fatigue constraint of variable amplitude load based on the equivalent static load approach

Seung Hyun Jeong[a], Jong Wook Lee[b], Gil Ho Yoon[b,*], Dong Hoon Choi[b]

[a] Construction Equipment Technology Center, Korea Institute of Industrial Technology (KITECH), Republic of Korea
[b] School of Mechanical Engineering, Hanyang University, Seoul, Republic of Korea

ARTICLE INFO

Article history:
Received 7 February 2017
Revised 25 October 2017
Accepted 12 December 2017
Available online 19 December 2017

Keywords:
Topology optimization
Fatigue constraints
Variable amplitude loading
Equivalent static load method

ABSTRACT

In this research, a new layout optimization method is developed to consider high cycle fatigue constraints which occur due to variable amplitude mechanical loading. Although fatigue is a very important property in terms of safety when designing mechanical components, it has rarely been considered in topology optimization with the lack of concept and the difficulty of sensitivity analysis for fatigue constraints calculated from multiaxial cycle counting. For the topology optimization for fatigue constraint, we use transient stress analysis to extract effective stress cycles and Miner's cumulative damage rule to calculate total damage at every spatial element. Because the calculation of the exact sensitivities of a transient system is complex and time consuming for the topology optimization application, this research proposes to use the pseudo-sensitivities of fatigue constraints calculated by applying equivalent static load approach. In addition, as an aggregated fatigue constraint is very sensitive to the changes in stress value which causes some unstable convergences in optimization process, a new scaling approach of the aggregated fatigue damage constraint is developed. To validate the usefulness of the developed approaches, we solved some benchmark topology optimization problems and found that the present method provides physically appropriate layouts with stable optimization convergence.

1. Introduction

In this research, a novel fatigue damage constraint topology optimization (TO) method is developed to consider high-cycle fatigue occurred by variable amplitude loading as shown in Fig. 1. The developed method uses stress histories at every finite element calculated from the transient finite element analysis of the Newmark method [1] and Miner's cumulative damage rule [2]. This research considers the fatigue model concerning high cycle fatigue in finite life region. For the calculation of fatigue constraint, the effective stress cycles are extracted by applying the multiaxial cycle counting method of Wang and Brown [2,3] and the fatigue constraint function was defined by the rule of Miner's linear cumulative damage based on the Basquin relation in conjunction with the Goodman correction. As a high cycle fatigue constraint is very sensitive to the changes in stress value which cause unstable convergence of the optimization process, pseudo-sensitivities calculated by applying equivalent static load (ESL) are developed and a new scaling approach of the aggregated fatigue damage constraint is

* Corresponding author.
E-mail address: ghy@hanyang.ac.kr (G.H. Yoon).

https://doi.org/10.1016/j.apm.2017.12.017
0307-904X/

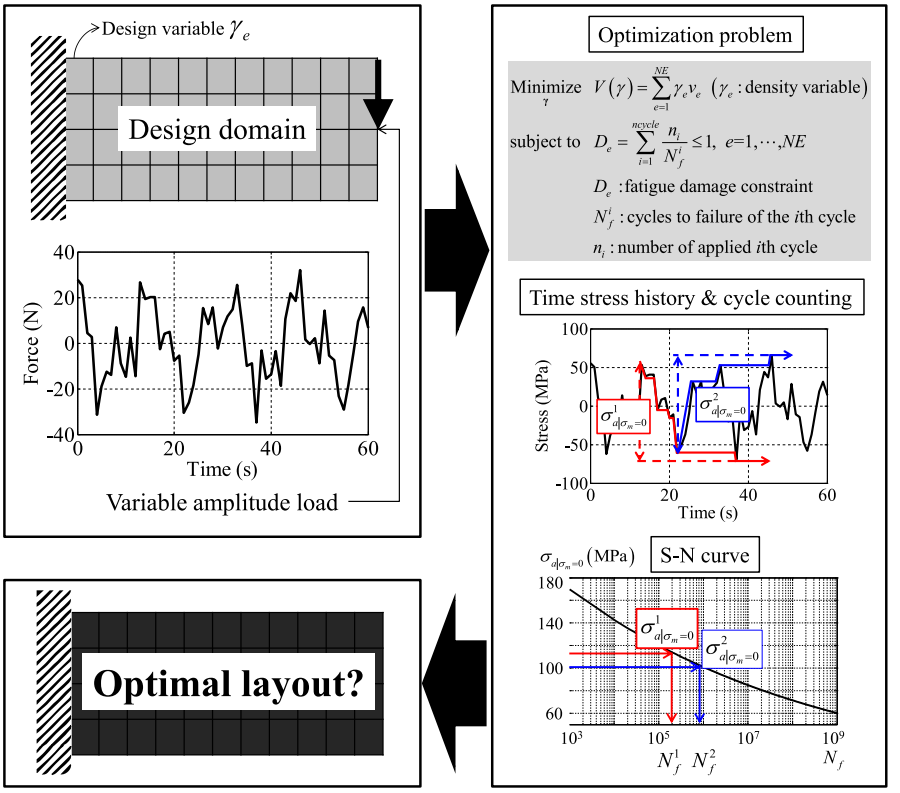

Fig. 1. The present fatigue damage constraint TO.

proposed. By solving some two-dimensional benchmark problems, the validity and the effectiveness of the present approach have been proven.

Despite the advancement in TO [4–8], it is still difficult to consider fatigue constraint in TO. After the concept of TO to minimize the strain energy of a structure with limited material usage was proposed [4,9,10], it has been applied to various kinds of design problems of mechanical components [11]. For example, the compliant mechanism design problem [12–15], the Eigen-frequency maximization design problem [16–22], and the stress-based design problem [23–27] have been considered by TO. Also, efficient topology optimization methods can be developed to resolve large-scale 3D problems [28,29]. The optimization methods considering multiaxial fatigue of machine components were proposed [30,31]. In recent years, the topology optimization methods considering the fatigue life constraint based on the time domain analysis have been proposed in Refs. [32–37]. The previous studies considered the stress history calculated from quasi-static analysis. The topology optimization considering fatigue life in the frequency domain was proposed in Refs. [38,39]. Unlike the previous research, we obtain the time stress history with the transient analysis based on the Newmark method. Thus the sensitivity analysis for transient system should be developed. As high-cycle fatigue uses the time stress history of a transient system, the three well-known difficulties related to the local stress constraint are naturally associated with this fatigue problem [23–27]. In addition to these difficulties, the sensitivity analysis of the cumulative fatigue constraint based on a complex multiaxial cycle counting method is highly sophisticated and has not been researched yet [40]. It is also found that the fatigue constraint is highly sensitive to changes in alternating and mean stress components. Generally, the graph of the S–N curve could be represented by the magnitude of a stress component against the logarithmic scale of cycles to failure [2]. Therefore, fatigue life changes significantly even with slight changes in stress value. It is a troublesome problem when trying to achieve stable optimization convergence. In this research, the challenge of sensitivity analysis of the damage constraint is solved by using a pseudo sensitivity analysis based on the equivalent static load (ESL) approach; the ESL approach is defined as the static load at each time step that generates the same displacement field with the transient system [41–45]. Although the sensitivities from the ESL are not exactly the same as the actual sensitivities of the transient system, we adopt a theory that the optimization results based on the ESL approach can satisfy Karush–Kuhn–Tucker (KKT) stationary conditions [43]. For a stable optimization convergence, the highly sensitive fatigue damage constraint can be relaxed by using a reasonable scaling approach.

1.1. Issues related to local fatigue damage constraint for TO

As the present TO method is based on high-cycle fatigue constraints using stress responses, the singularity problem, the local constraint problem, and the highly nonlinear behavior are basically inherited [23–27]. At first, the singularity problem occurs for the TO method using solid isotropic material with penalization (SIMP) [23,25,26]. In the SIMP method, the design variables are relaxed to have a range from a small positive value to simulate the void region to one to simulate the solid region. Due to the small positive value of the lower bound, a stress value of an element does not become zero, although the design variable of that element approaches its lower bound to simulate the void region. As a result, a gradient-based optimizer suffers when finding an optimal material distribution. There are many resolutions proposed recently to cope with the singularity problem. The epsilon-relaxed stress [23] and the *qp*-relaxation [24,25,46] are well known approaches to solve the singularity problem. The *qp*-relaxation uses different penalization parameters to interpolate Young's modulus for structural analysis and Young's modulus for stress evaluation [24,25]. Secondly the local constraint problem occurs because the stress constraint is a local property and should be imposed for every FE element. If the number of elements increases, the computational cost for sensitivity analysis and optimization becomes huge; therefore we cannot find an optimal solution within a reasonable computational time [25,26,47,48]. To cope with this issue, the *p*-norm function and the Kreisselmeier–Steinhauser (KS) function can be applied [25,26,47,48]. These functions aggregate element stress values and approximate the maximum stress value. Although these approaches cannot exactly represent the real maximum value, the computational cost for sensitivity analysis and optimization can be dramatically reduced. The highly non-linear behavior of the stress constraint occurred when design variables are relaxed and the global constraint approach is employed. To cope with this problem, an accurate and efficient gradient-based optimizer should be developed. In this research, the numerical issues related to the stress-constrained TO problem for a static structural load are also observed and numerical techniques developed for the stress-constrained TO are applied.

1.2. Difficulty of sensitivity analysis in a transient system

In this research, the fatigue damage constraint is based on the multiaxial cycle counting method extracting effective *alternating* and *mean* stress cycles for the cumulative damage constraint. This implies that the sensitivities of the cumulative damage constraint for the specific effective time steps also should be derived and calculated during an optimization process. As the sensitivity analysis of transient system is a complex and time consuming process, there is a huge computational cost to implement it for the gradient-based TO [41–45]. The present research proposes to use the equivalent static load approach for the TO of the transient system. To our knowledge, although it has some theoretical drawbacks, the ESL approach has been applied for some kinds of structural design problems for linear and nonlinear transient systems [41–45]. The main advantage of the ESL approach in various problems lies in its simple implementation for TO with a reasonable computational cost [41–45]. In addition the ESL approach can be easily implemented into tailored finite element codes because it relies on the pseudo adjoint sensitivity analysis of static loads to obtain sensitivity values. Indeed to obtain the pseudo sensitivity values for the fatigue damage constraint easily and to determine a proper physical layout after the TO easily, the concept of an ESL approach is our natural choice. Also we validated the proposed pseudo sensitivity analysis by comparing it with the FDM analysis in a simple two-bar size optimization example. From the example, we found that the pseudo sensitivity value is not exactly the same as the value of FDM, but the differences between them decrease and converge during the optimization. It is also possible to check whether the optimization results using the pseudo sensitivity value satisfy the stationary KKT condition as proved in the previous research [43]. The results and discussions are included in the numerical example section.

1.3. Highly sensitive fatigue damage constraint

In the high-cycle fatigue theory, the graph of S–N curve could be represented by the magnitude of a stress component against the logarithmic scale of cycles to failure. The high-cycle fatigue life generally ranges from 10^4 to 10^6 or to 10^7 for finite life region. As the scale in fatigue life is very large, we found that it is very sensitive to the changes in the stress components. Due to this highly sensitive behavior of the fatigue damage constraint, the value of the constraint fluctuates severely during optimization. Due to these fluctuations, a gradient-based optimizer cannot converge stably. To cope with this difficulty, we proposed an appropriate scaling method of the original Basquin equation. By employing the new scaling approach of the fatigue constraint, the gradient-based optimizer converges and reasonable topology optimized layouts can be obtained.

This paper consists of the following four sections. In the second section, a detailed formulation of the TO considering fatigue constraints is presented. The scaled cumulative damage constraints of the mechanical structure under variable amplitude loads are considered for the prevention of fatigue. In the third section, the equivalent static load approach for pseudo sensitivity analysis of the fatigue damage constraint will be described. In the fourth section, some illustrative design optimization examples including a simple two-bar, an L-shaped beam, and cantilever beam were solved with the present fatigue constraints. In particular, after comparing the results of the two-bar size optimization and the two-bar TO, the validity and limitations of the present fatigue-constrained TO method were discussed. Also we investigate the effect of scale

factor of damage constraint by solving the L-shaped beam and cantilever beam problem. Finally, some concluding remarks are discussed in the final section.

2. Fatigue constrained TO formulation

2.1. Original fatigue constrained TO formulation

In the fatigue constrained TO problem, the total material volume is minimized subject to the fatigue damage constraint as follows:

$$\begin{aligned} &\underset{\gamma}{\text{Minimize}} && V(\gamma) = \sum_{e=1}^{NE} \gamma_e v_e \\ &\text{subject to} && D_e \le 1, \qquad e = 1, \cdots, NE \end{aligned} \tag{1}$$

where γ_e, v_e, and D_e represent the eth element density design variable of the SIMP method, the element volume, and the fatigue damage of the eth element, respectively. This formulation is similar to the stress-based TO which minimizes volume subject to local stress constraints. To our best knowledge, it is rare to consider the element wise dynamic failure constraint. Similar to the element stress constraints in the stress-based topology optimization, the fatigue damage constraints are also local constraints and should be satisfied for all elements; therefore, the number of constraints is the same as the number of elements, NE. To effectively consider these local fatigue damage constraints with a gradient based optimizer, the TO formulation should be reformulated by the concept of the global constraint.

2.2. Fatigue analysis procedure

Before developing the detailed procedures of the TO using the global constraint approach, this section briefly introduces the fatigue analysis procedure for variable amplitude loading. The fatigue life is commonly calculated by considering the alternating and the mean stresses of an effective cycle extracted from the transient stress history as shown in Fig. 2. First, the transient stress history of a dynamic system is calculated by a transient finite element analysis or quasi static analysis. Based on the calculation of the transient stress history, the effective loading cycle can be extracted by an appropriate cycle counting method such as the uniaxial rainflow cycle counting and the multiaxial cycle counting method by Wang and Brown [2,3]. For the variable amplitude multiaxial loading, there are two common approaches for the fatigue analysis. One is the critical plane approach and the other is the equivalent stress or strain approach. In the critical plane approach, the fatigue damage parameter of each potential plane is calculated using uniaxial cycle counting and the critical plane can be identified. In the equivalent stress or strain approach, the fatigue damage parameter is defined based on the cumulative equivalent stress or strain value from a multiaxial rainflow reversal counting method [2]. From an analysis point of view, the fatigue constraint of each criterion can be calculated according to the well-developed analysis process. From an optimization point of view, it becomes a very difficult problem because of some non-differentiable operations of fatigue analysis. For example, with the critical plane approach, the process for finding critical plane becomes non-differentiable because the critical plane changes during the optimization iterates. Therefore, we adopt the equivalent stress approach based on the multiaxial cycle counting method and Basquin relation to consider the transient stress history in a multiaxial stress state. After the calculation of load cycle, the cumulative damage rule is applied by considering the alternating and the mean stresses of the effective cycle [2,3,49].

2.2.1. Transient finite element analysis

We obtain the stress history of a given dynamic system by solving the following equation of motion:

$$\mathbf{M}\ddot{\mathbf{u}}(t) + \mathbf{D}\dot{\mathbf{u}}(t) + \mathbf{K}\mathbf{u}(t) = \mathbf{F}(t) \tag{2}$$

where **M, D, K, F**(t), and $\mathbf{u}(t)$ represent the consistent global mass matrix, the global damping matrix, the global stiffness matrix, the time dependent force vector and the corresponding displacement vector, respectively. The first and second order derivatives of the displacement vector with respect to time are denoted as $\dot{\mathbf{u}}(t)$ and $\ddot{\mathbf{u}}(t)$, respectively. The initial condition of displacement, velocity, and acceleration are all zero unless stated otherwise.

The global stiffness and the global mass matrices are constructed by assembling the eth element stiffness matrix, $\mathbf{k}_e$, and the eth element mass matrix, $\mathbf{m}_e$, respectively as follows.

$$\mathbf{K} = \mathop{\mathbf{A}}_{e=1}^{NE} \mathbf{k}_e \text{ with } \mathbf{C}_e = \gamma_e^n \mathbf{C}_0, \ \mathbf{k}_e = \int_{v_e} \mathbf{B}^{\mathrm{T}} \mathbf{C}_e \mathbf{B} dv \ (: e\text{th element domain}) \tag{3}$$

$$\mathbf{M} = \mathop{\mathbf{A}}_{e=1}^{NE} \mathbf{m}_e \text{ with } \mathbf{m}_e = \gamma_e^{n_m} \mathbf{m}_0, \ \mathbf{m}_0 = \int_{v_e} \rho \mathbf{N}^{\mathrm{T}} \mathbf{N} dv \ (: e\text{th element domain}) \tag{4}$$

where $\mathbf{B}$ and $\mathbf{C}_e$ represent the strain-displacement matrix and the constitutive matrix, respectively. The constitutive matrix without interpolation is denoted by $\mathbf{C}_0$ and the FE assembly operator is denoted by $\mathbf{A}$. The material density and the shape function of the eth element are denoted by ρ and $\mathbf{N}$, respectively. The penalization parameter of the Young's modulus is

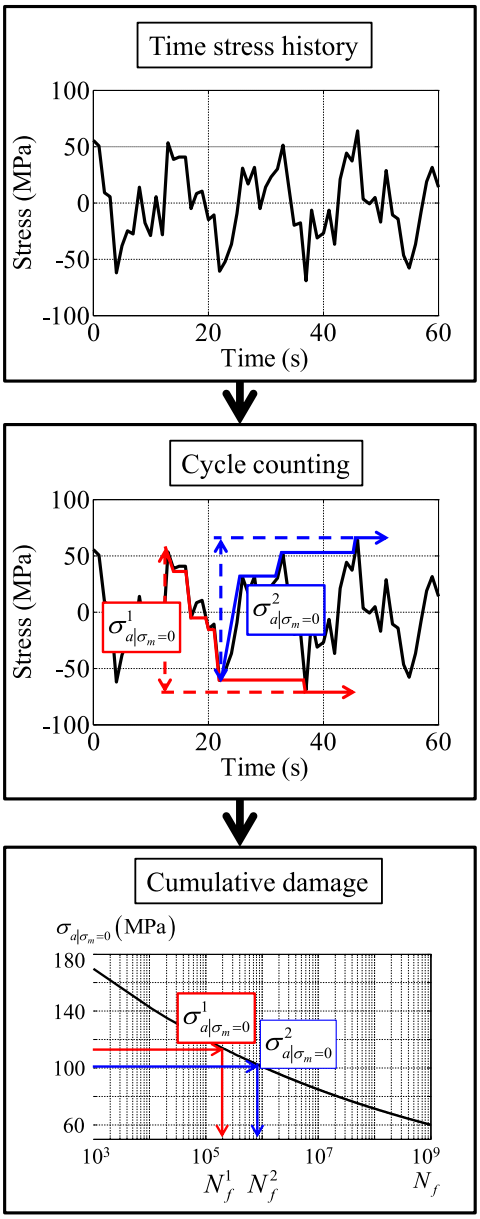

Fig. 2. A brief illustration of the fatigue analysis procedure.

denoted by n. From the previous studies, the value of n is important to create a black-and-white design and is fixed at 3 in this research [9,10]. Furthermore, it is important that the mass penalization parameter, n_m, should be larger than the value of the Young's modulus penalization parameter, n, to avoid the local mode problem [10]; therefore the value of n_m is fixed at 4 in this research. For the damping matrix, **D**, Rayleigh damping is used, which uses a linear combination of the global mass and stiffness matrices as follows:

$$\mathbf{D} = a\mathbf{M} + b\mathbf{K} \tag{5}$$

To solve the dynamic Eq. (2), we use the implicit direct integration, known as the Newmark method which calculates a response history with step-by-step integration in time [1]. After obtaining the displacement time history, we can evaluate the element stress vector of the eth element at the $n+1$ time step by using the following equation.

$$\boldsymbol{\sigma}_{e,n+1} = {}_S\mathbf{C}_e\mathbf{B}\mathbf{u}_{e,n+1} \tag{6}$$

where ${}_S\mathbf{C}_e$ is the constitutive matrix for the stress evaluation and calculated by using the following equation. The eth element displacement vector and the associate stress are $\mathbf{u}_{e,n+1}$ and $\boldsymbol{\sigma}_{e,n+1}$, respectively.

$${}_S\mathbf{C}_e = \gamma_e^{n_s}\mathbf{C}_0 \tag{7}$$

In Eq. (7), the penalization parameter for the stress evaluation is denoted by n_s. From the relevant researches on the stress-based TO, it is known that the value of n_s plays an important role in avoiding a stress singularity problem [24–26]. Based on the previous researches, the value of n_s is fixed at 0.5 here. The resultant stress history is used to extract an effective fatigue cycle by using the multiaxial cycle counting method.

2.2.2. Multiaxial cycle counting method

For a complicated multiaxial load time history, there are two techniques to assess the fatigue damage of a structure. The first approach, i.e., the critical plane approach, segregates the material volume into candidate planes and applies the uniaxial cycle counting method to calculate the fatigue damage on each candidate plane. The plane that accumulates the most damage is deemed to be the critical plane. The second approach, i.e., the equivalent stress amplitude method, uses a multiaxial cycle counting technique which assumes that the fatigue damage or life can be evaluated from the cycles identified from the complicated equivalent stress history. A general multiaxial reversal counting technique was developed by Wang and Brown [2,3]. The detailed procedure is as follows:

Step 1. From the stress histories, calculate the equivalent stress time history based on the von Mises criterion as follows.

$$\sigma(t) = \sqrt{\sigma_x^2(t) + \sigma_y^2(t) - \sigma_x(t)\sigma_y(t) + 3\tau_{xy}^2(t)} \tag{8}$$

Step 2. Reorder the stress history to begin with the time point, t_0, that has the maximum amplitude of equivalent stress.
Step 3. Calculate the relative equivalent stress time history as follows.

$$\Delta\sigma(t) = \sqrt{\Delta\sigma_x^2(t) + \Delta\sigma_y^2(t) - \Delta\sigma_x(t)\Delta\sigma_y(t) + 3\Delta\tau_{xy}^2(t)} \tag{9}$$

where

$$\Delta\sigma_x(t) = \sigma_x(t) - \sigma_x(t_0),\ \Delta\sigma_y(t) = \sigma_y(t) - \sigma_y(t_0),\ \Delta\tau_{xy}(t) = \tau_{xy}(t) - \tau_{xy}(t_0) \tag{10}$$

Step 4. Collect all points that cause $\Delta\sigma(t)$ to increase. The collected points belong to the first major reversal.
Step 5. Store the remaining points which can be gathered as one or more blocks that start and end with the same value of $\Delta\sigma(t)$ and a trailing block.
Step 6. For each uncounted block, set the first point as the reference point and calculate the relative equivalent stress. Proceed to collect points that cause the new $\Delta\sigma(t)$ to increase. This process finds additional reversals and possibly more uncounted blocks.
Step 7. Repeat step 6 until all the data are collected.

Because we count effective reversals with the multiaxial cycle counting, the number of cycles of counted reversals is one half in this method.

2.2.3. Fatigue damage calculation based on Miner's rule

After the effective cycles are identified, the fatigue damage due to each cycle is calculated by considering the mean and alternating stress effect and the cumulative fatigue damage rule is applied. On the ith cycle, we can calculate the alternating stress and mean stress by using the following equation [2,3,49].

$$\boldsymbol{\sigma}_{a,i} = \begin{bmatrix}\sigma_{a,x} & \sigma_{a,y} & \tau_{a,xy}\end{bmatrix} = \frac{\boldsymbol{\sigma}_{\max,i} - \boldsymbol{\sigma}_{\min,i}}{2} \tag{11}$$

$$\boldsymbol{\sigma}_{m,i} = \begin{bmatrix}\sigma_{m,x} & \sigma_{m,y} & \tau_{m,xy}\end{bmatrix} = \frac{\boldsymbol{\sigma}_{\max,i} + \boldsymbol{\sigma}_{\min,i}}{2} \tag{12}$$

where $\boldsymbol{\sigma}_{a,i}$ and $\boldsymbol{\sigma}_{m,i}$ represent the alternating and mean element stress vector of the ith cycle. The first and last stress vectors of the ith cycle are denoted by $\boldsymbol{\sigma}_{\min,i}$ and $\boldsymbol{\sigma}_{\max,i}$, respectively. With the calculated alternate and mean stress vectors, the equivalent alternating and mean stresses, $\sigma_{a,i}$ and $\sigma_{m,i}$, can be calculated by using the following equation.

$$\sigma_{a,i} = \sqrt{\sigma_{a,x}^2 + \sigma_{a,y}^2 - \sigma_{a,x}\sigma_{a,y} + 3\tau_{a,xy}^2} \tag{13}$$

$$\sigma_{m,i} = \sigma_{m,x} + \sigma_{m,y} \tag{14}$$

Now, we should relate the alternating and mean stress of each cycle with the total fatigue damage using Miner's rule. First, we relate the magnitude of the alternating and mean stress with the magnitude of the alternating stress without mean

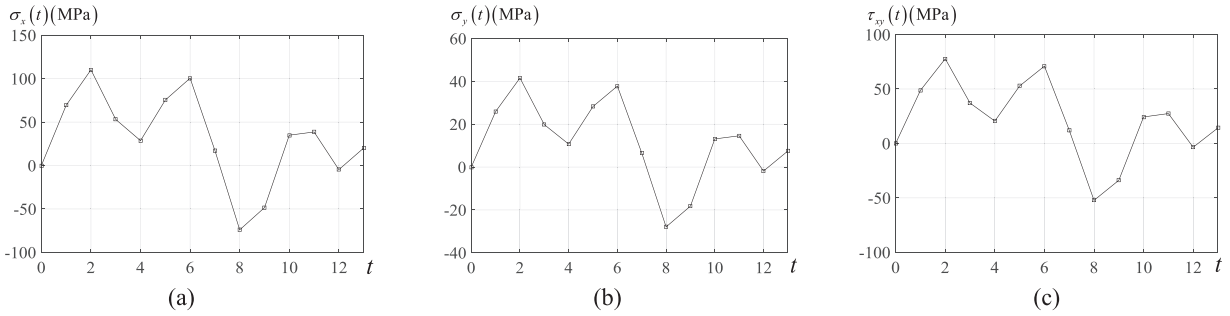

Fig. 3. An example of time stress history.

stress by using the modified Goodman criterion, which is a theory of mean stress correction, formulated as follows [2,3,49].

$$\sigma_{a|\sigma_m=0,i} = \frac{\sigma_{a,i}}{1 - \frac{\sigma_{m,i}}{S_{ut}}} \tag{15}$$

where the alternating stress without mean stress effect of the ith cycle and the ultimate tensile strength are denoted by $\sigma_{a|\sigma_m=0,i}$ and S_{ut}, respectively. The compressive mean stress does not affect fatigue damage, therefore Eq. (15) is modified as follows [2,3,49].

$$\sigma_{a|\sigma_m=0,i} = \frac{\sigma_{a,i}}{1 - \frac{\max(\sigma_{m,i},0)}{S_{ut}}} \tag{16}$$

Now, we can calculate the number of cycles to failure of the ith cycle, N_i, by using the Basquin equation as follows.

$$\sigma_f (2N_i)^{b_f} = \sigma_{a|\sigma_m=0,i} \tag{17}$$

where σ_f and b_f are the fatigue strength coefficient and the exponent of the Basquin equation, respectively. By rearranging Eq. (17) and substituting Eq. (16) into (17), we can represent the number of cycles to failure of the ith cycle,N_i, by using the alternating and mean stress as follows.

$$N_i = \frac{1}{2}\left(\frac{S_{ut}\sigma_{a,i}}{\sigma_f(S_{ut} - \max(\sigma_{m,i},0))}\right)^{\frac{1}{b_f}} \tag{18}$$

By using N_i, the cumulative damage can be calculated according to Miner's rule as follows.

$$D = \sum_{i=1}^{ncycle} D_i = \sum_{i=1}^{ncycle} \frac{n_i}{N_i} \tag{19}$$

where n_i is the number of ith cycles applied. To avoid fatigue, the cumulative damage D should be lower than 1.

2.2.4. Simple example of fatigue life calculation

This subsection presents a simple illustrative fatigue analysis example. Let's assume that the transient FE analysis is conducted and the time stress history is obtained as shown in Fig. 3. The ultimate tensile strength (S_{ut}) in (18), the fatigue strength (σ_f), and the exponent of the Basquin equation (b_f) in (17) are set to 380 MPa, 650 MPa, and −0.075, respectively. The desired minimum life is set to 10^5. Because the equivalent stress is maximized at $t=2$, the time stress history is reordered to start at $t=2$ by following the cycle counting procedure in the step 2. The reordered time history is denoted by t_{rel}. At the step 3, the relative equivalent time stress history can be obtained as shown in Fig. 4(a). If we collect all data points that cause the relative equivalent stress to increase, the data points in the reordered time ranges from $t_{rel}=0$ to $t_{rel}=2$ and from $t_{rel}=5$ to $t_{rel}=6$ can be collected and regarded as the first cycle time range. Now, the uncounted block includes the data points in the time range from $t_{rel}=2$ to $t_{rel}=4$ and from $t_{rel}=6$ to $t_{rel}=13$. By following step 6, we set the first data point of the uncounted block, the point at $t_{rel}=2$, as the new reference point and calculate the new relative equivalent stress time history as shown in Fig. 4(b). As the relative equivalent time stress history increases from $t_{rel}=2$ to $t_{rel}=4$, these blocks are counted as the second cycle time range. Because there is the uncounted data in the time history, step 6 is repeated until all data points are counted as shown in Fig. 4(c–f). Finally, 6 effective cycles are counted from this example. From the counted effective cycle, we can calculate the magnitude of alternating stress, mean stress, and the corresponding damage of each cycle as shown in Table 1. In this simple example, the total damage is 2.78×10^{-4}. Therefore fatigue does not occur.

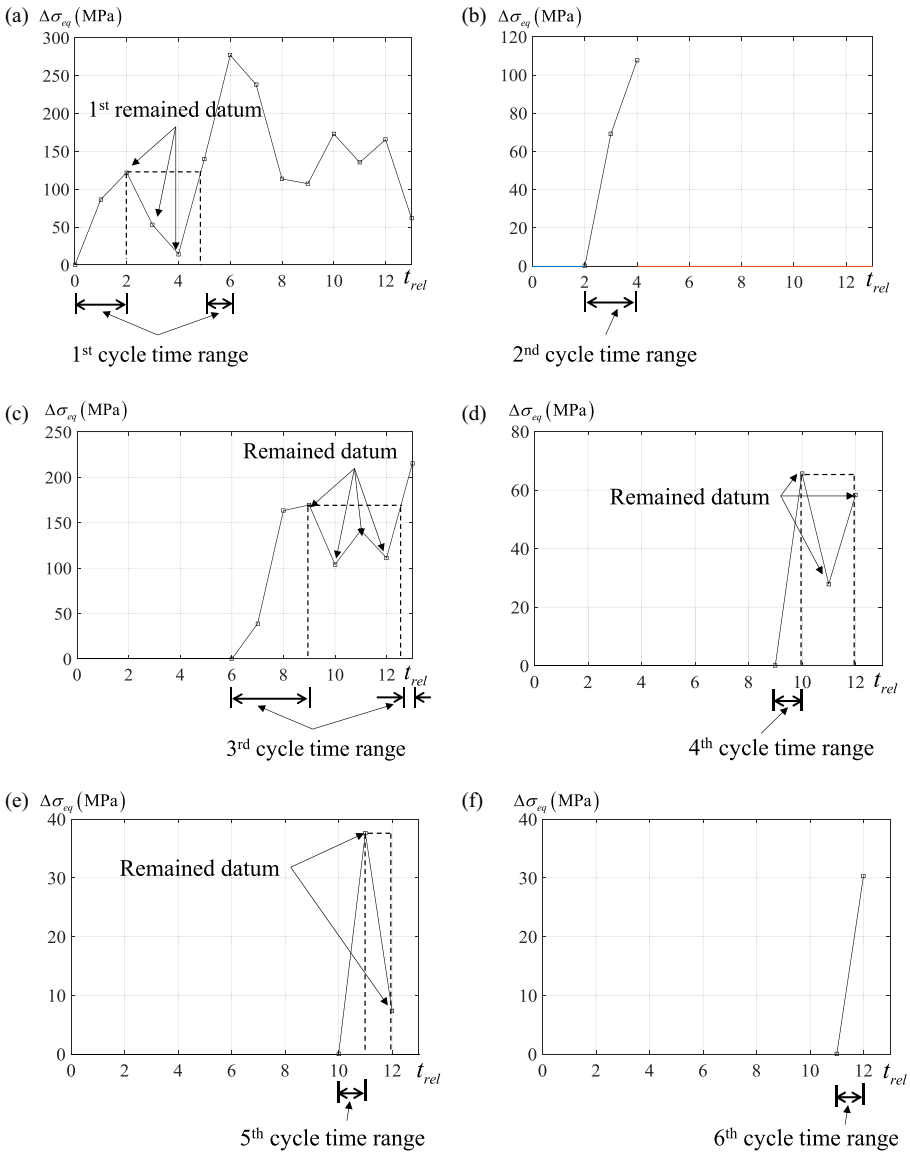

Fig. 4. An example of multiaxial cycle counting.

Table 1
Magnitude of alternating stress, mean stress, and damage from each cycle.

	n_i	$\sigma_{a,i}$ (MPa)	$\sigma_{m,i}$ (MPa)	N_i	D_i
1	10^5	138.46	24.896	1.82×10^3	2.74×10^{-4}
2	10^5	53.841	88.836	3.81×10^7	1.31×10^{-8}
3	10^5	107.66	−3.3782	1.29×10^5	3.88×10^{-6}
4	10^5	32.808	23.314	4.21×10^{11}	1.19×10^{-12}
5	10^5	18.835	10.517	1.10×1015	4.53×10^{-16}
6	10^5	15.172	13.816	1.75×10^{16}	2.86×10^{-17}
Total damage					2.78×10^{-4}

2.3. TO reformulation

By using the above analysis procedure, the responses of the original TO can be calculated. However, there are various numerical difficulties that must be resolved in order to solve the original TO problem. First of all, the damage constraint is highly sensitive to small changes in stress and the maximum operator between two values is not differentiable. Moreover,

due to the alternating and mean stress used for the calculation of fatigue damage, the singularity problem and local constraint problem are basically inherited. Therefore, the following subsections describe the proposed approach to cope with these problems.

2.3.1. Reformulation of the damage constraint

In the damage constraint (19), the maximum operator between the values of mean stress and zero should be differentiable to use a gradient-based optimizer. Therefore, the differentiable maximum operator between two variables is defined by using the following equation [10].

$$\max(\sigma_m, 0) \approx \Psi_{2,\max}(\sigma_m, 0) = \frac{\sigma_m}{2} + \frac{\sqrt{{\sigma_m}^2 + \varepsilon}}{2} \approx \begin{cases} \sigma_m & \sigma_m \geq 0 \\ 0 & \sigma_m < 0 \end{cases} \tag{20}$$

Also, the value of b_f in (17) is generally from −0.05 to −0.1 for most metals [49]. Because the reciprocal of b_f is used as the exponent, the damage is highly sensitive to the changes in the alternating and mean stress. Inevitably this problem affects the optimization procedure. We found that a gradient-based optimizer similar to that used in the method of moving asymptotes (MMA) [50] sometimes cannot find a local optimum. To cope with this numerical issue, we reformulate the fatigue damage constraint by scaling the fatigue damage constraint function. Let us recall the fatigue damage constraint, which is represented by using the alternating and mean stresses as follows:

$$D = \sum_{i=1}^{ncycle} D_i = \sum_{i=1}^{ncycle} \frac{n_i}{N_i} = \sum_{i=1}^{ncycle} 2n_i \left(\frac{S_{ut}\sigma_{a,i}}{\sigma_f(S_{ut} - \Psi_{2,\max}(\sigma_{m,i}, 0))} \right)^{-\frac{1}{b_f}} \leq 1 \tag{21}$$

Then for the optimization, the original fatigue damage constraint is reformulated by using the scale factor, *SF*, as follows.

$$\tilde{D} = D^{\frac{1}{SF}} = \left(\sum_{i=1}^{ncycle} 2n_i \left(\frac{S_{ut}\sigma_{a,i}}{\sigma_f(S_{ut} - \Psi_{2,\max}(\sigma_{m,i}, 0))} \right)^{-\frac{1}{b_f}} \right)^{\frac{1}{SF}} \leq 1 \tag{22}$$

The above proposed fatigue damage constraint function can give smooth damage distribution in design domain according to the changes in alternating and mean stress values when an appropriate value is used. Thus we expect that a gradient-based optimizer converges to a stable point. The convergence history of the optimizer using the original and the proposed fatigue damage constraint function will be compared in the numerical example section.

2.3.2. TO formulation using the p-norm constraint

Since the present TO treats the local fatigue damage constraint calculated from the alternating and mean stresses, the singularity and the local constraint problems are basically inherited. Therefore, the present method adopts the density filtering approach and the *p*-norm constraint approach, which are known to work well for the stress-based TO. Finally the original TO problem in (1) is reformulated as follows.

$$\begin{aligned} &\underset{\gamma}{\text{Minimize}} \quad V(\tilde{\gamma}) = \sum_{e=1}^{NE} \tilde{\gamma}_e v_e \quad (\tilde{\gamma} : \text{Filtered density}) \\ &\text{subject to} \quad \left\langle \tilde{D}_{\max} \right\rangle_k \leq 1, \qquad k = 1, \cdots, NR \\ &\qquad\qquad \tilde{\gamma} = \Xi(\gamma) \text{ with the denstiy filter } \Xi \end{aligned} \tag{23}$$

$$\left\langle \tilde{D}_{\max} \right\rangle_k = \max\left(\tilde{D}_e\right), \qquad \text{if } e \in \Omega \text{ and the } e\text{th element exists} \tag{24}$$

Here, the design variable of the *e*th element, γ_e, is changed into the filtered design variable, $\tilde{\gamma}_e$. The local damage constraints with the number of *NE* are changed by using the maximum operator, $\langle \tilde{D}_{\max} \rangle_k$. With the maximum operator, the number of constraints can be drastically decreased from *NE* to the number of subdomains, *NR*. To make the maximum operator differentiable, the *p*-norm constraint is used in this research and formulated as follows.

$$\left\langle \tilde{D}_{\max} \right\rangle_k = c_k^{iter} \left\langle \tilde{D}_{PN} \right\rangle_k, \ (e \in \Omega_k) \tag{25}$$

$$\left\langle \tilde{D}_{PN} \right\rangle_k \equiv \left(\sum_e (\tilde{D}_e)^p \tilde{\gamma}_e \right)^{1/p}, \ (e \in \Omega_k) \tag{26}$$

$$c_k^{iter} = \tau \frac{\tilde{D}_{k,\max}^{iter-1}}{\left\langle \tilde{D}_{PN} \right\rangle_k^{iter-1}} + (1-\tau) c_k^{iter-1}, \qquad 0 < \tau < 1 \tag{27}$$

In Eqs. (25) and (27), the correction parameter, c_k^{iter}, is determined by using the ratio between the value of the *p*-norm constraint and the value of the maximum fatigue damage of the previous iteration with the damping parameter, τ, which is used to avoid oscillations of the constraint. As the optimizer converges, the ratio between the value of the *p*-norm constraint and the value of the maximum constraint also converges; therefore the original local constraints will be satisfied for all elements.

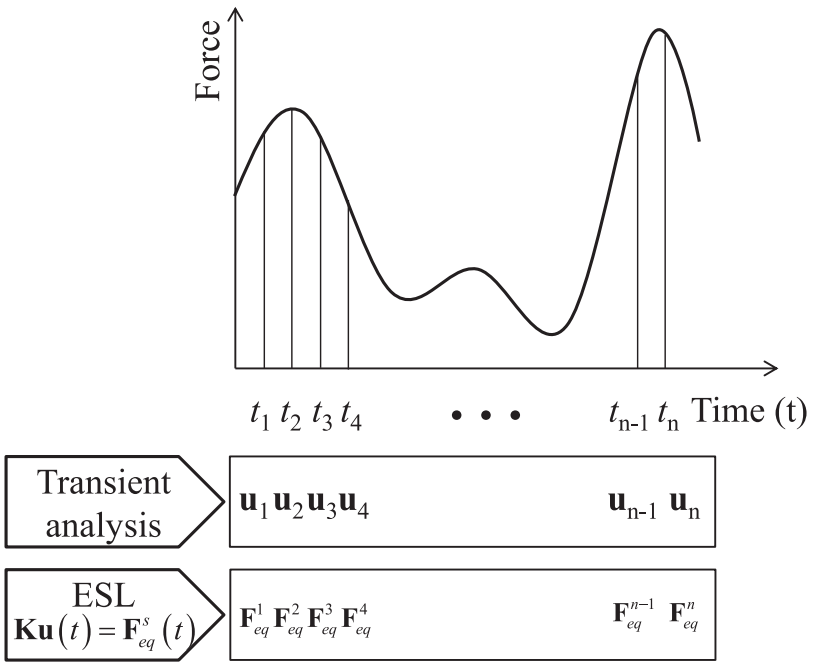

Fig. 5. The definition of the equivalent static load.

3. Pseudo sensitivity analysis through equivalent static load

To treat the *p*-norm fatigue damage constraint by a gradient-based optimizer such as the sequential quadratic programming, the method of moving asymptotes (MMA) [50], or convex linearization (CONLIN) [51], the sensitivities of the *p*-norm constraint should be provided. However, determining the sensitivities of a transient response is a very complex process [41–45] and it takes a long time. Indeed we employ the equivalent static load (ESL) approach to simplify the sensitivity analysis and to reduce the computational cost of the TO process. A detailed description of ESL and the pseudo sensitivity analysis are provided in this section.

3.1. The equivalent static load of a dynamic transient system

Despite some drawbacks in the theory, the ESL approach has been applied for the TO problem for linear and nonlinear dynamic systems [41–45]; the purpose of the present study is not the supporting the theory but an engineering approach to utilize the ESL approach in the transient analysis is presented. This method has been implemented inside the commercial topology optimization software of Optistruct and Genesis. According to some relevant researches, the equivalent static load can be defined as load vectors which generate the same displacement field at each time step of the transient system [41–45]. Consider the governing equation of the dynamic system again and its corresponding equivalent static load as follows:

$$\mathbf{M\ddot{u}}(t)+\mathbf{D\dot{u}}(t)+\mathbf{Ku}(t)=\mathbf{F}(t) \tag{28}$$

$$\mathbf{Ku}(t)=\mathbf{F}^s_{eq}(t) \tag{29}$$

where the equivalent static load of time step t is denoted by $\mathbf{F}^s_{eq}(t)$. The definition of ESL is given in Fig. 5.

Through the definition of ESL, the displacement at time t obtained by the ESL at time t is exactly the same as the displacement obtained by transient analysis. Mathematically the sensitivity obtained by the ESL at time t is not exactly the same as the sensitivity of the transient system. It is insisted that if the optimizations are iteratively conducted and the optimization converges, the difference between exact sensitivity and pseudo sensitivity becomes small enough; the proof of this statement is beyond the scope of this research and we just accept this insist [41–45]. Finally, the obtained solution satisfies the Karush–Kuhn–Tucker (KKT) necessary conditions [43]. The appropriateness of the proposed approach is verified in the numerical example section.

3.2. Pseudo sensitivity analysis

As we employ the ESL to obtain the pseudo sensitivity for dynamic fatigue damage, the followings can be derived by using the chain rule as follows:

$$\frac{d\langle \tilde{D}_{PN}\rangle_k}{d\gamma_e} = \frac{\partial\langle \tilde{D}_{PN}\rangle_k}{\partial\gamma_e} + \frac{\partial\langle \tilde{D}_{PN}\rangle_k}{\partial\tilde{D}_e}\sum_{i=1}^{ncycle}\left(\frac{\partial\tilde{D}_e}{\partial\sigma_{a,i}}\frac{\partial\sigma_{a,i}}{\partial\boldsymbol{\sigma}_{a,i}}\frac{\partial\boldsymbol{\sigma}_{a,i}}{\partial\gamma_e} + \frac{\partial\tilde{D}_e}{\partial\sigma_{m,i}}\frac{\partial\sigma_{m,i}}{\partial\boldsymbol{\sigma}_{m,i}}\frac{\partial\boldsymbol{\sigma}_{m,i}}{\partial\gamma_e}\right)$$
$$+ \sum_{e'\in\Omega_k}\frac{\partial\langle \tilde{D}_{PN}\rangle_k}{\partial\tilde{D}_{e'}}\sum_{i=1}^{ncycle}\left(\frac{\partial\tilde{D}_{e'}}{\partial\sigma_{a,i}}\frac{\partial\sigma_{a,i}}{\partial\boldsymbol{\sigma}_{a,i}}\frac{\partial\boldsymbol{\sigma}_{a,i}}{\partial\mathbf{u}_{a,i}}\frac{d\mathbf{u}_{a,i}}{d\gamma_{e'}} + \frac{\partial\tilde{D}_{e'}}{\partial\sigma_{m,i}}\frac{\partial\sigma_{m,i}}{\partial\boldsymbol{\sigma}_{m,i}}\frac{\partial\boldsymbol{\sigma}_{m,i}}{\partial\mathbf{u}_{m,i}}\frac{d\mathbf{u}_{m,i}}{d\gamma_{e'}}\right) \tag{30}$$

To obtain the pseudo sensitivity of the alternating and mean displacement vectors, $\mathbf{u}_{a,i}$ and $\mathbf{u}_{m,i}$, respectively, the sensitivity of ith cycle's maximum and minimum displacement vectors can be used as follows:

$$\frac{d\mathbf{u}_{a,i}}{d\gamma_e} = \frac{1}{2}\left(\frac{d\mathbf{u}_{\max,i}}{d\gamma_e} - \frac{d\mathbf{u}_{\min,i}}{d\gamma_e}\right) \tag{31}$$

$$\frac{d\mathbf{u}_{m,i}}{d\gamma_e} = \frac{1}{2}\left(\frac{d\mathbf{u}_{\max,i}}{d\gamma_e} + \frac{d\mathbf{u}_{\min,i}}{d\gamma_e}\right) \tag{32}$$

where the ith cycle's first and last displacement vectors are denoted by $\mathbf{u}_{\min,i}$ and $\mathbf{u}_{\max,i}$, respectively. By using the corresponding ESL of the first and last time steps of the ith cycle, the pseudo sensitivity of $\mathbf{u}_{\min,i}$ and $\mathbf{u}_{\max,i}$ can be derived as follows.

$$\frac{d\mathbf{u}_{\max,i}}{d\gamma_e} \cong -\mathbf{K}^{-1}\frac{d\mathbf{K}}{d\gamma_e}\mathbf{u}_{\max,i} \tag{33}$$

$$\frac{d\mathbf{u}_{\min,i}}{d\gamma_e} \cong -\mathbf{K}^{-1}\frac{d\mathbf{K}}{d\gamma_e}\mathbf{u}_{\min,i} \tag{34}$$

By substituting the Eqs. (33) and (34) into (30), the pseudo sensitivity of the p-norm damage constraint can be derived as follows.

$$\frac{d\langle \tilde{D}_{PN}\rangle_k}{d\gamma_e} \cong \frac{\partial\langle \tilde{D}_{PN}\rangle_k}{\partial\gamma_e} + \frac{\partial\langle \tilde{D}_{PN}\rangle_k}{\partial\tilde{D}_e}\sum_{i=1}^{ncycle}\left(\frac{\partial\tilde{D}_e}{\partial\sigma_{a,i}}\frac{\partial\sigma_{a,i}}{\partial\boldsymbol{\sigma}_{a,i}}\frac{\partial\boldsymbol{\sigma}_{a,i}}{\partial\gamma_e} + \frac{\partial\tilde{D}_e}{\partial\sigma_{m,i}}\frac{\partial\sigma_{m,i}}{\partial\boldsymbol{\sigma}_{m,i}}\frac{\partial\boldsymbol{\sigma}_{m,i}}{\partial\gamma_e}\right)$$
$$+ \frac{1}{2}\sum_{e'\in\Omega_k}\frac{\partial\langle \tilde{D}_{PN}\rangle_k}{\partial\tilde{D}_{e'}}\sum_{i=1}^{ncycle}\left(\frac{\partial\tilde{D}_{e'}}{\partial\sigma_{a,i}}\frac{\partial\sigma_{a,i}}{\partial\boldsymbol{\sigma}_{a,i}}\frac{\partial\boldsymbol{\sigma}_{a,i}}{\partial\mathbf{u}_{a,i}} + \frac{\partial\tilde{D}_{e'}}{\partial\sigma_{m,i}}\frac{\partial\sigma_{m,i}}{\partial\boldsymbol{\sigma}_{m,i}}\frac{\partial\boldsymbol{\sigma}_{m,i}}{\partial\mathbf{u}_{m,i}}\right)\left(-\mathbf{K}^{-1}\frac{d\mathbf{K}}{d\gamma_e}\mathbf{u}_{\max,i}\right)$$
$$+ \frac{1}{2}\sum_{e'\in\Omega_k}\frac{\partial\langle \tilde{D}_{PN}\rangle_k}{\partial\tilde{D}_{e'}}\sum_{i=1}^{ncycle}\left(-\frac{\partial\tilde{D}_{e'}}{\partial\sigma_{a,i}}\frac{\partial\sigma_{a,i}}{\partial\boldsymbol{\sigma}_{a,i}}\frac{\partial\boldsymbol{\sigma}_{a,i}}{\partial\mathbf{u}_{a,i}} + \frac{\partial\tilde{D}_{e'}}{\partial\sigma_{m,i}}\frac{\partial\sigma_{m,i}}{\partial\boldsymbol{\sigma}_{m,i}}\frac{\partial\boldsymbol{\sigma}_{m,i}}{\partial\mathbf{u}_{m,i}}\right)\left(-\mathbf{K}^{-1}\frac{d\mathbf{K}}{d\gamma_e}\mathbf{u}_{\min,i}\right) \tag{35}$$

The sensitivity of the p-norm fatigue damage constraint finally can be calculated by using the adjoint variables as follows.

$$\frac{d\langle \tilde{D}_{PN}\rangle_k}{d\gamma_e} \cong \frac{\partial\langle \tilde{D}_{PN}\rangle_k}{\partial\gamma_e} + \frac{\partial\langle \tilde{D}_{PN}\rangle_k}{\partial\tilde{D}_e}\sum_{i=1}^{ncycle}\left(\frac{\partial\tilde{D}_e}{\partial\sigma_{a,i}}\frac{\partial\sigma_{a,i}}{\partial\boldsymbol{\sigma}_{a,i}}\frac{\partial\boldsymbol{\sigma}_{a,i}}{\partial\gamma_e} + \frac{\partial\tilde{D}_e}{\partial\sigma_{m,i}}\frac{\partial\sigma_{m,i}}{\partial\boldsymbol{\sigma}_{m,i}}\frac{\partial\boldsymbol{\sigma}_{m,i}}{\partial\gamma_e}\right)$$
$$- \sum_{i=1}^{ncycle}\lambda_{\max,i}^T\frac{d\mathbf{K}}{d\gamma_e}\mathbf{u}_{\max,i} - \sum_{i=1}^{ncycle}\lambda_{\min,i}^T\frac{d\mathbf{K}}{d\gamma_e}\mathbf{u}_{\min,i} \tag{36}$$

$$\mathbf{K}\lambda_{\max,i} = \frac{1}{2}\sum_{e'\in\Omega_k}\frac{\partial\langle \tilde{D}_{PN}\rangle_k}{\partial\tilde{D}_{e'}}\left(\frac{\partial\tilde{D}_{e'}}{\partial\sigma_{a,i}}\frac{\partial\sigma_{a,i}}{\partial\boldsymbol{\sigma}_{a,i}}\frac{\partial\boldsymbol{\sigma}_{a,i}}{\partial\mathbf{u}_{a,i}} + \frac{\partial\tilde{D}_{e'}}{\partial\sigma_{m,i}}\frac{\partial\sigma_{m,i}}{\partial\boldsymbol{\sigma}_{m,i}}\frac{\partial\boldsymbol{\sigma}_{m,i}}{\partial\mathbf{u}_{m,i}}\right)^T$$
$$\mathbf{K}\lambda_{\min,i} = \frac{1}{2}\mathbf{K}^{-1}\sum_{e'\in\Omega_k}\frac{\partial\langle \tilde{D}_{PN}\rangle_k}{\partial\tilde{D}_{e'}}\left(-\frac{\partial\tilde{D}_{e'}}{\partial\sigma_{a,i}}\frac{\partial\sigma_{a,i}}{\partial\boldsymbol{\sigma}_{a,i}}\frac{\partial\boldsymbol{\sigma}_{a,i}}{\partial\mathbf{u}_{a,i}} + \frac{\partial\tilde{D}_{e'}}{\partial\sigma_{m,i}}\frac{\partial\sigma_{m,i}}{\partial\boldsymbol{\sigma}_{m,i}}\frac{\partial\boldsymbol{\sigma}_{m,i}}{\partial\mathbf{u}_{m,i}}\right)^T \tag{37}$$

In this sensitivity analysis, the ESL vectors of each cycle's time steps occurring maximum and minimum stress values are needed for the adjoint sensitivity analysis. Therefore the present method is effective compared with the method using the exact sensitivity value of transient system because it uses the equivalent static loads for the sensitivity analysis.

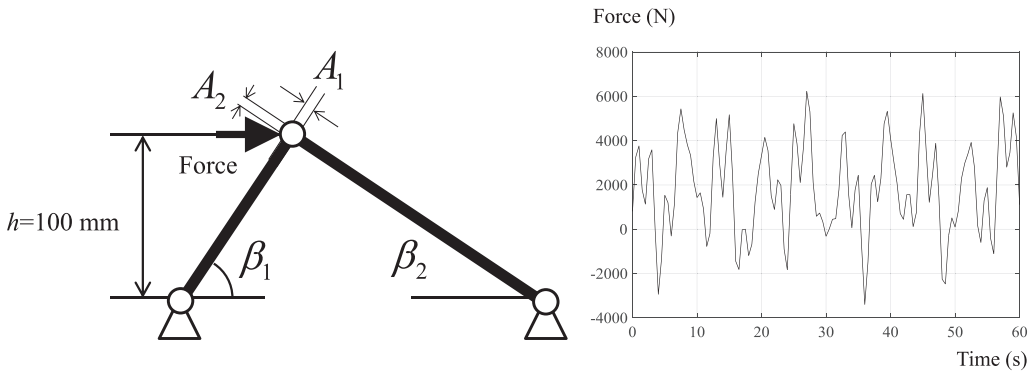

Fig. 6. Two-bar configuration and history of fluctuating force.

4. TO examples for fatigue damage constraint

To demonstrate the effectiveness and validity of the present TO method, this section solves three optimization problems: the two-bar design, the L-shaped beam design problem, and a cantilever beam design. The two-bar size optimization problem considering the fatigue constraint is solved to investigate the validity of the present study. The time step size is set to 0.5 s for all examples unless stated otherwise. Especially, the sensitivity analysis approach with the pseudo sensitivities based on the ESL for the size optimization problem is compared with the finite difference method. Also we check the KKT necessary condition for each iteration of the size optimization. For the design optimization, the method of moving asymptotes (MMA) [50] is used.

4.1. Example 1: Two bar design optimization

The two-bar design optimization problem is considered for the first numerical example. This example was used in the previous research to validate the usefulness of TO by comparing it with the size optimization result for the Drucker–Prager yield condition. This research modifies the size optimization problem to consider the fatigue constraint that occurs due to the variable amplitude load. An optimization process finishes if the value of maximum change in the design variable between two sequential optimization iterations is smaller than 0.001 or the iteration number is larger than the maximum iteration number, 100. Since the time required for one optimization iteration is 24 s, it takes 2400 s until the end of 100 iterations.

4.1.1. Two dimensional two-bar design by size optimization

From the size optimization, we can validate the present pseudo sensitivity analysis of the fatigue constraint. As mentioned in the Section 3.1, it was proved mathematically that the differences between exact sensitivity values and pseudo sensitivity values from ESL are converged to some value after design optimization [43]. So here we check the difference in actual sensitivity using a finite difference method (FDM) and the pseudo sensitivity using an ESL approach during design optimization for the two-bar size optimization problem. Also we check to see whether the optimization result satisfies the KKT necessary conditions as proved mathematically in previous research [43]. The configuration of two-bar and the time history of the variable amplitude load of the size optimization problem are presented in Fig. 6. Young's modulus and the material density are set to $E = 200$ GPa and $\rho = 7860$ Kg, respectively. The ultimate tensile strength (S_{ut}) in (18), the fatigue strength (σ_f), and the exponent of the Basquin equation (b_f) in (17) are set to 380 MPa, 650 MPa, and -0.075, respectively. The desired minimum life is set to 10^5, 10^6, and 10^7 for three design cases applied by the fluctuating forces shown in Fig. 6. The fluctuating force shown in Fig. 6 is applied 10^5, 10^6, and 10^7 times for each design case, respectively. The two-bar is discretized by two truss elements and the design variables are cross sectional areas of two bars (A_1 and A_2) and angles of two bars (β_1 and β_2). Transient analysis for obtaining the time stress history is performed by using the stiffness, mass and damping matrices in (38) and (39). We solve the size optimization problem stated in (40).

$$\mathbf{k}_e = \frac{EA_e}{l_e}\begin{bmatrix} c^2 & cs & -c^2 & -cs \\ cs & s^2 & -cs & -s^2 \\ -c^2 & -cs & c^2 & cs \\ -cs & -s^2 & cs & s^2 \end{bmatrix},\ \mathbf{m}_e = \frac{\rho A_e l_e}{6}\begin{bmatrix} 2 & 0 & 1 & 0 \\ 0 & 2 & 0 & 1 \\ 1 & 0 & 2 & 0 \\ 0 & 1 & 0 & 2 \end{bmatrix},\ \sigma_e = \frac{E}{l_e}[-c \quad -s \quad c \quad s]\mathbf{u}_e \tag{38}$$

$$\mathbf{D} = a\mathbf{M} + b\mathbf{K},\ a = 0.08,\ b = 0.06 \tag{39}$$

$$\begin{aligned} &\underset{A_1,A_2,\beta_1,\beta_2}{\text{Minimize}} && V(A_1, A_2, \beta_1, \beta_2) = \left(\tfrac{A_1}{\sin\beta_1} + \tfrac{A_2}{\sin\beta_2}\right)h \\ &\text{subject to} && D_e \le 1, \qquad e = 1, 2 \end{aligned} \tag{40}$$

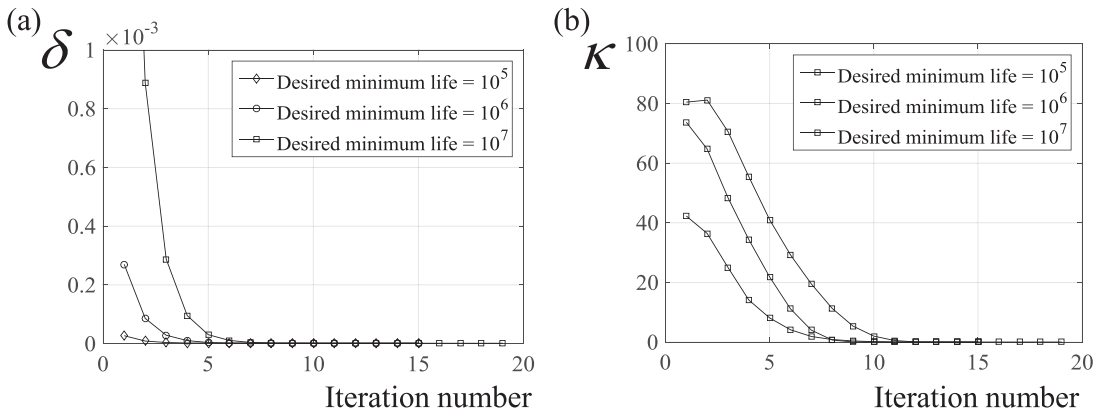

Fig. 7. Maximum differences between the analytical sensitivities and the KKT stationary condition during the optimization processes for three loading design cases with the different desired minimum life. (a) Maximum difference between FDM and the pseudo sensitivity analysis through ESL and (b) the value of KKT stationary condition.

Table 2
The difference between two sensitivities and the KKT necessary condition for three design cases.

Iteration number	δ			κ		
	Desired life = 10^5	Desired life = 10^6	Desired life = 10^7	Desired life = 10^5	Desired life = 10^6	Desired life = 10^7
1	2.70×10^{-5}	2.70×10^{-4}	2.71×10^{-3}	4.23×10^{1}	7.37×10^{1}	8.05×10^{1}
2	8.85×10^{-6}	8.60×10^{-5}	8.88×10^{-4}	3.64×10^{1}	6.47×10^{1}	8.12×10^{1}
3	3.81×10^{-6}	2.86×10^{-5}	2.88×10^{-4}	2.50×10^{1}	4.84×10^{1}	$7.06 \times 10^{-}$
...	...	...	...	...	...	...
17	1.82×10^{-6}	1.53×10^{-6}	1.27×10^{-6}	9.31×10^{-5}	2.31×10^{-5}	1.38×10^{-3}
18	1.89×10^{-6}	1.59×10^{-6}	1.36×10^{-6}	4.02×10^{-5}	6.51×10^{-6}	2.63×10^{-4}
19			1.34×10^{-6}			1.15×10^{-4}
20			1.33×10^{-6}			3.91×10^{-5}
21			1.30×10^{-6}			2.65×10^{-5}
			1.37×10^{-6}			1.76E-05

As we mentioned, we check the accuracy of the sensitivity values and the KKT condition during the design optimization. The maximum difference in sensitivity obtained by FDM and pseudo sensitivity analysis is calculated as follows.

$$\delta = \max_{e=1,2} \left| \left(\frac{dD_e}{d\mathbf{x}} \right)_{FDM} - \left(\frac{dD_e}{d\mathbf{x}} \right)_{ESL} \right|, \ \mathbf{x} = [A_1\, A_2\, \beta_1\, \beta_2] \tag{41}$$

where the sensitivity vectors calculated by using the FDM and the pseudo sensitivity analysis are denoted by $(\frac{dD_e}{d\mathbf{x}})_{FDM}$ and $(\frac{dD_e}{d\mathbf{x}})_{ESL}$, respectively. Also, the KKT stationary condition can be stated as follows:

$$\kappa = \left\| \nabla V(\mathbf{x}) + \sum_{e=1}^{2} \mu_e \nabla D_e \right\| \tag{42}$$

where∇V, ∇D_e and, μ_e represent the gradient vector of volume, the gradient vector of the eth element damage, and the Lagrange multiplier of the eth constraint, respectively. Because we calculate Euclidean norm, κ in Eq. (42) is a scalar value. Fig. 7(a) presents histories of δ and κ during the design optimization for the three design cases. As illustrated, the KKT stationary condition is satisfied after the design optimizations. The differences in the sensitivity value converge to small values for all design cases as the number of iterations increases as shown in Table 2. The design optimization results are summarized in Table 3. Because of the different effects of tensile and compressive stresses, the cross sectional area and angle are different. However, it is interesting that the volume of each bar is the same although the cross sectional area and angle are different. By observing the design optimization results and the convergence history of δ and κ, we can validate the appropriateness of the pseudo sensitivity analysis based on the ESL for the fatigue constraint optimization problem.

4.1.2. Two dimensional two-bar design by TO

In addition to the size optimization, we solve the two-bar TO problem. The material properties are the same as in the size optimization problem. The ultimate tensile strength, the fatigue strength, the exponent of the Basquin equation, and the desired minimum life are also the same as in the size optimization problem. Fig. 8 presents the design domain and fluctuating force history of the TO problem. The force is distributed to five nodes as shown in Fig. 8 and the rectangular design domain, 400 mm by 100 mm, is discretized by 120 by 30 linear QUAD plane stress elements. The thickness of the

Table 3
Two-bar size optimization result.

Iteration number	Optimal design variables		
	Desired life = 10^5	Desired life = 10^6	Desired life = 10^7
A_1 (mm^2)	11.819	13.733	16.017
A_2 (mm^2)	10.732	12.665	14.963
β_1 (deg)	47.759	47.317	46.949
β_2 (deg)	42.241	42.683	43.051
V_1 (mm^3)	1.596×10^3	1.868×10^3	2.192×10^3
V_2 (mm^3)	1.596×10^3	1.868×10^3	2.192×10^3

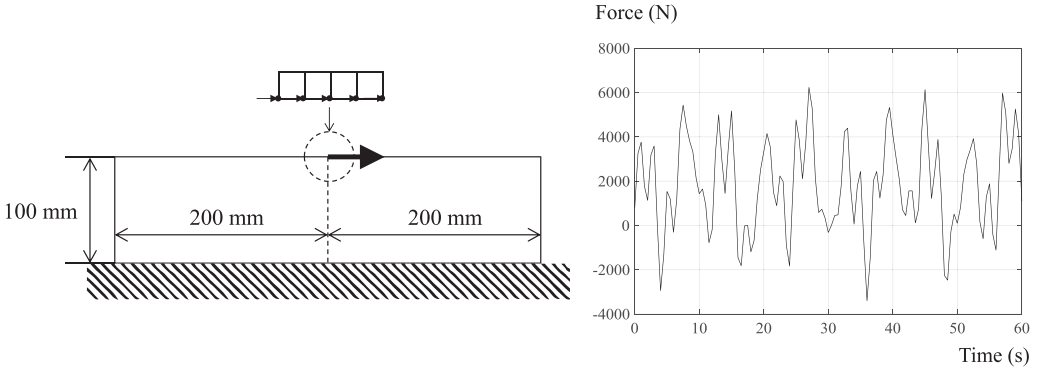

Fig. 8. Design domain of two-bar TO and history of fluctuating force.

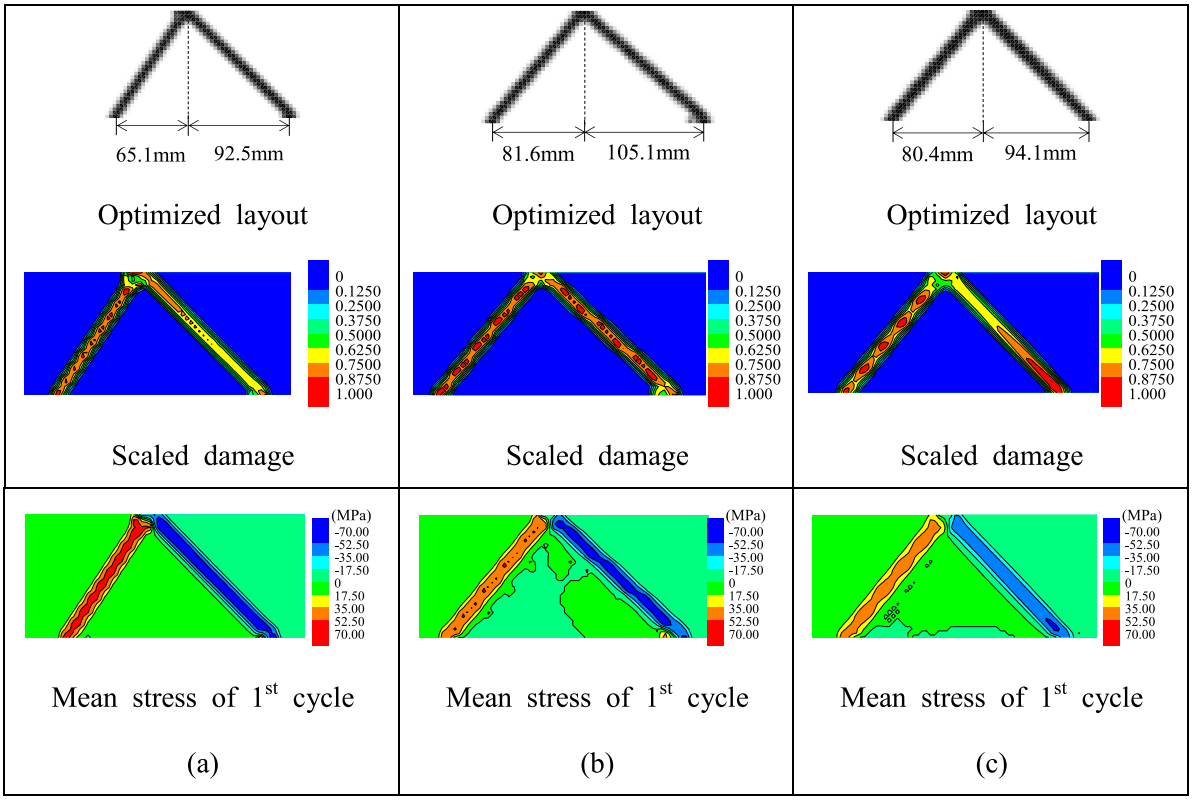

Fig. 9. Optimized layouts according to the desired life obtained by proposed TO: (a) desired life = 10^5, (b) desired life = 10^6, and (c) desired life = 10^7.

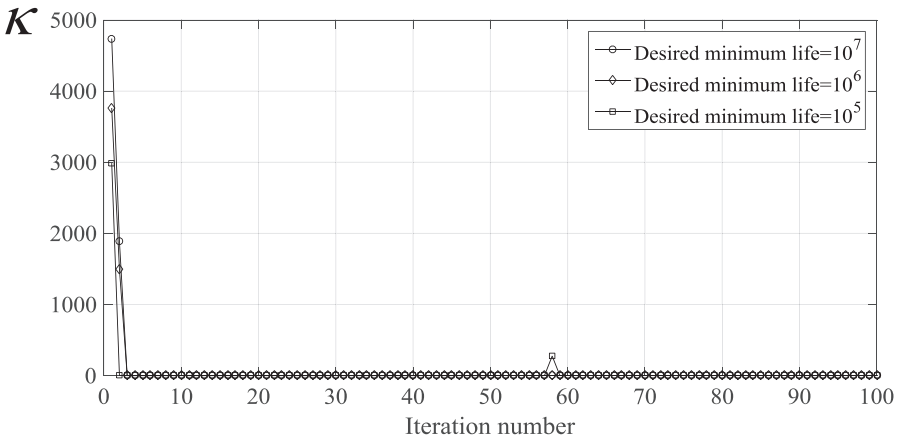

Fig. 10. The KKT necessary condition for three design cases of TO results.

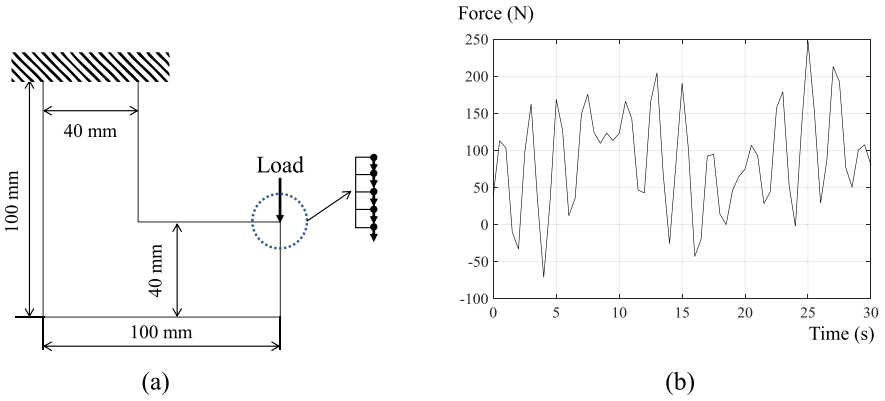

Fig. 11. The L-shaped beam problem: (a) design domain, boundary condition, applied loading position, and (b) a history of the mechanical force.

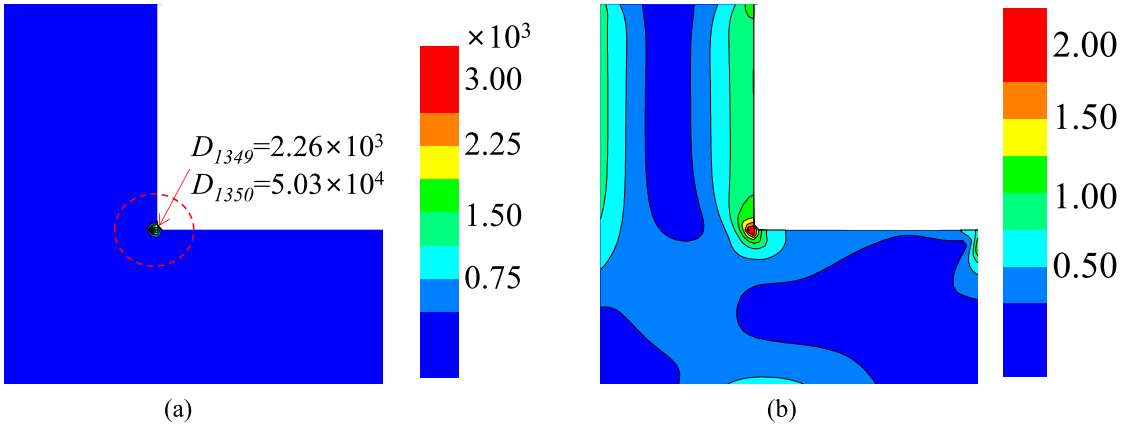

Fig. 12. Localization problem according to the scale factor when the design variables are set to 0.65: (a) the contour of un-scaled damage and (b) the contour of scaled damage when the scale factor is set to 12.

element is 2.5 mm and the lower edge of the design domain is fixed. For the TO, the number of regions for p-norm, NR, is set to 4 and the p value of p-norm is fixed at 4. See some relevant researches for the effect of NR and p value [52,53].

Fig. 9 presents the optimized layouts of the two-bar design problem according to some desired minimum fatigue lives. As in the simple layout of the size optimization problem, two bars appear through the present TO. Through the optimization, the volume fraction, V/V_0, where $V_0 = \sum_{e=1}^{NE} v_e$, is increased to 0.060, 0.065, and 0.073 and the maximum value of fatigue damage is 1.01 0.98, and 1.00 for the desired life 10^5, 10^6, and 10^7, respectively; therefore the constraints are satisfied for all cases. Similar with the size optimization, we check the KKT necessary condition for the TO results. Fig. 10 represents the

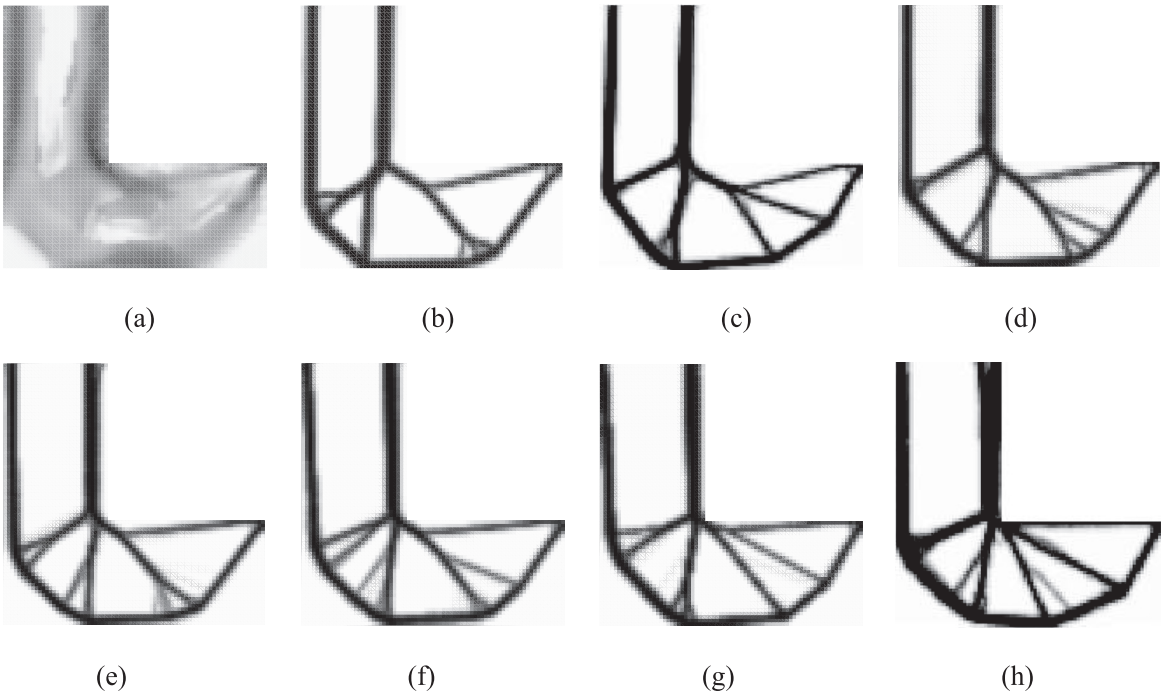

Fig. 13. Optimization result with respect to the scale factor: (a) scale factor = 6 (not converged), (b) scale factor = 8 ($V/V_0 = 0.291$, $D_{max} = 0.95$), (c) scale factor = 10 ($V/V_0 = 0.277$, $D_{max} = 1.02$), (d) scale factor = 12 ($V/V_0 = 0.271$, $D_{max} = 0.95$), (e) scale factor = 14 ($V/V_0 = 0.266$, $D_{max} = 1.02$), (f) scale factor = 16 ($V/V_0 = 0.271$, $D_{max} = 1.04$), (g) scale factor = 18 ($V/V_0 = 0.277$, $D_{max} = 0.95$) and (h) scale factor = 20 ($V/V_0 = 0.343$, $D_{max} = 1.07$).

Table 4
A comparison of the designs by the two-bar size optimization and the TO.

	Size optimization result			TO result		
	Desired life = 10^5	Desired life = 10^6	Desired life = 10^7	Desired life = 10^5	Desired life = 10^6	Desired life = 10^7
β_1 (deg)	47.759	47.317	46.949	≈ 56.936	≈ 50.786	≈ 51.200
β_2 (deg)	42.241	42.683	43.051	≈ 47.231	≈ 43.576	≈ 46.741
V_1 (mm^3)	1.596×10^3	1.868×10^3	2.192×10^3	1.083×10^3 (39 elements)	1.472×10^3 (53 elements)	2.000×10^3 (72 elements)
V_2 (mm^3)	1.596×10^3	1.868×10^3	2.192×10^3	1.750×10^3 (63 elements)	1.861×10^3 (67 elements)	2.250×10^3 (81 elements)
Total volume	3.192×10^3	3.736×10^3	4.384×10^3	2.833×10^3	3.333×10^3	4.250×10^3

convergence history of the KKT necessary condition, κ, during the design optimization. From the convergence history, it is observed that the present TO method based on the ESL approach satisfies the KKT necessary condition because the value of κ converges to zero for all cases. In Fig. 10, a sudden change of κ occurs when the desired minimum life is set to 10^5. This is due to a sudden increase of the Lagrange multiplier calculated from the MMA optimizer. In addition, to compare the topology optimized result with the size optimization result, the angle and the volume of each bar are compared in Table 4. The angle of each bar is calculated by using the horizontal length of each bar shown in Fig. 9. The volume of each bar is calculated by considering the value of the density and the mean stress of the first loading cycle in Fig. 9. As shown in Fig. 9, the tensile mean stress is applied to the left bar at the first cycle. Therefore we regard the element with $\tilde{\gamma}_e > 0.85$ and $\sigma_{m,1} > 0$ as the members of the left bar. For the other case, if there is an element with $\tilde{\gamma}_e > 0.85$ and$\sigma_{m,1} < 0$, we regard it as the member of the right bar. We count the elements of the two bars by using the described criteria and calculate the volume of each bar by multiplying the volume of an element. As shown in Table 4, it is observed that the angles are slightly different. Two bars of the TO result tends to be narrower because two angles are smaller than those of the size optimization result. Also the volume of each bar is different between the two results. The volume of the left bar of the TO result is smaller than that of the size optimization result and the volume of the right bar of the TO result is larger than that of the size optimization result. The total volume of two bars in the TO result is larger than that of the size optimization result. The difference between the two optimization approaches occurs due to different optimization problem formulations. Because there are too many design variables in the TO, the p-norm constraints are used instead. The result of TO tends to be localized compared with the size optimization result. With a design domain with complex boundary conditions, the present TO approach is valuable for determining the initial configuration of the structure. From the two-bar design optimization example, we can validate the usefulness and limitations of the present approach.

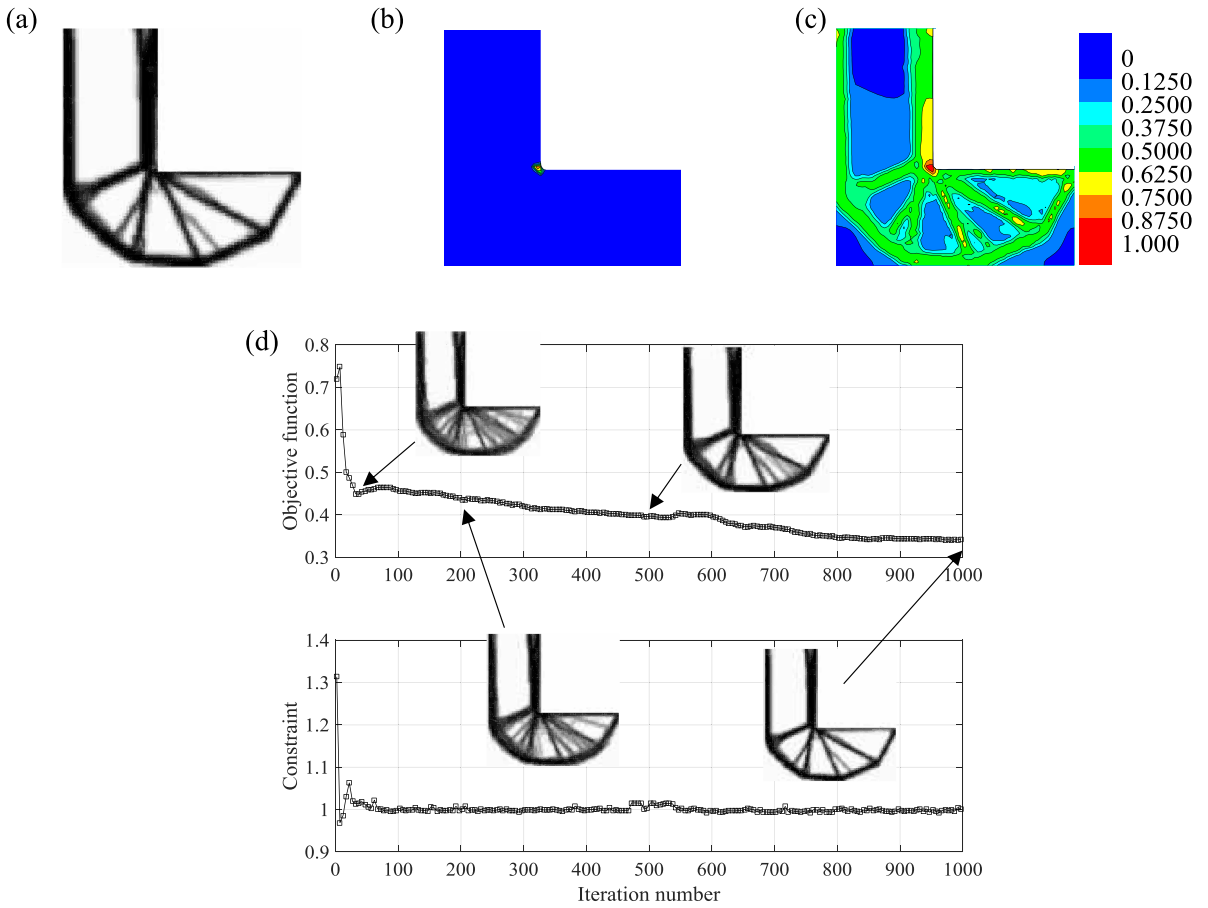

Fig. 14. Optimized shape and the damage distribution of the result using the scaled damage (scale factor = 20): (a) the optimized shape ($V/V_0 = 0.343$), (b) the distribution of the un-scaled damage ($D_{max} = 1.07$), (c) the distribution of the scaled damage ($\tilde{D}_{\max} = 1.00$), (d) the convergence history of the objective function and constraint.

4.2. Example 2: L-shaped beam

For the next example, an L-shaped beam is considered. The design domain, the clamped boundary condition, and the applied loading are shown in Fig. 11. The design domain is discretized by the 3600 1.3 mm by 1.3 mm quadrilateral Q4 plane stress elements. The thickness of an element is set to 1 mm. The number of regions for p-norm calculation is set to 1. The value of p for the p-norm calculation is set to 4. Young's modulus, Poisson's ratio, and density are set to 210 GPa, 0.3, and 7820 kg/m^3, respectively. And the desired minimum value for life is set to 10^6. To calculate the fatigue damage, the ultimate tensile strength in (18), S_{ut}, the fatigue damage strength coefficient, σ_f, and the exponent of the Basquin equation, b_f, in (17) are set to 380 MPa, 650 MPa, and −0.075, respectively. In this example, we especially test the validity of present fatigue damage scaling approach. An optimization process finishes if the value of maximum change in the design variable between two sequential optimization iterations is smaller than 0.001 or the iteration number is larger than the maximum iteration number, 2000. Since the time required for one iteration is 16.2 s, it takes 32,400 s to complete the 2000 iterations.

To solve the fatigue constraint topology optimization problems, we introduce the modified fatigue damage constraint concept in Section 2. In this section, we present the reason of using the modified fatigue damage constraint. At the Section 2, we mentioned that if the fatigue damage isn't scaled, the localization problem can occur due to highly nonlinear distribution of damage constraint. The localization problem according to the scale factor is presented in Fig. 12.

In Fig. 12, the design variables are set to 0.65 in the design domain. Here we observe that the fatigue damage has the largest value, near to 5×10^4, in a specific region (a dashed circle in the Fig. 12(a)) but almost fatigue damage has zero values in the other regions without the scaling of the fatigue damage. The largest damage value, 5.03×10^4, is obtained at the 1350th element. The damage value near to the 1350th element, the 1349th element, is 2.26×10^3. The alternating stresses of the 1st effective cycle of the 1350th element and the 1349th element are 478.4 MPa and 333.8 MPa, respectively. The mean stresses of the 1st effective cycle of the 1350th element and the 1349th element are 7.182 MPa and 4.058 MPa, respectively. Although the difference of the 1st effective cycle's alternating stress between the 1350th and the 1349th elements is 144.6 MPa, the difference of damage between the 1350th and the 1349th elements is 5.00×10^4. Due to the logarithmic

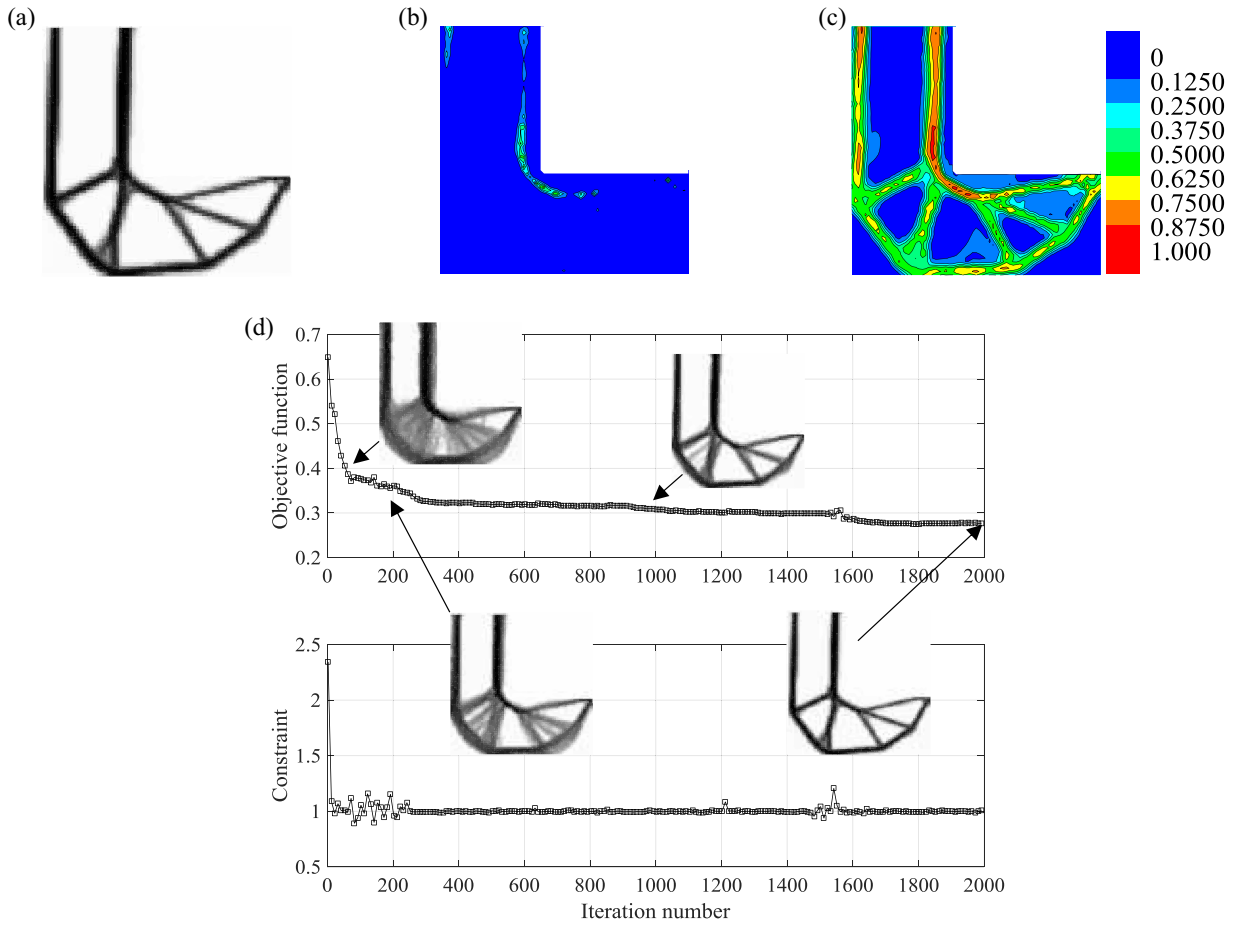

Fig. 15. Optimized shape and the damage distribution of the result using the scaled damage (scale factor = 10): (a) the optimized shape ($V/V_0 = 0.277$), (b) the distribution of the un-scaled damage ($D_{max} = 1.02$), (c) the distribution of the scaled damage ($\tilde{D}_{\max} = 1.00$), (d) the convergence history of the objective function and the constraint.

relation between stress and cycles to failure, small changes of alternating and mean stress can result in large changes of cycles to failure. In this research, this phenomenon is called as localization problem because it affects to convergence of the optimization procedure. To resolve this problem, the modified fatigue damage constraint concept using the scale factor is presented in (22). Through the modified fatigue damage formulation, we can get the more smoothed damage distribution when we set the value of scale factor to 12 as shown in Fig. 12(b). However, we must find the best value for the scale factor for the modified fatigue damage because the scale factor is newly introduced value in this research. Because it isn't introduced by mathematical demonstration, it must be fined by trial and error. Many cases are considered and their results are presented in Fig. 13.

With a small value for the scaling parameter, it is hard to obtain the stable convergence as Fig. 13(a). With a too large value for the scaling parameter, a smoothed reentrance corner cannot be achievable as Fig. 13(h).

The maximum fatigue damage is presented at the reentrant corner when the scale factor is higher than 18. This phenomenon occurs because the stress concentration is relaxed more than necessary. As shown in Fig. 14, the optimization result considering fatigue constraint is similar with the compliance minimization result with 20 for the value of scale factor. However, the stress concentration can be relaxed due to the round corner with scale factors smaller than 10 as shown in Fig. 15. From the results, we can conclude that an appropriate value of scale factor is very import to get the clear shape and avoid stress concentration.

By Figs. 14 and 15, we can confirm that the scale factor affect to the optimized result and the higher value of the scale factor cannot resolve the stress concentration phenomenon because it relaxes the stress concentration more than necessary. That is, an appropriate value of scale factor must be used to get more clear shape and to resolve the localization problem.

In Fig. 16, the effect of time step size for the topology optimization is tested. The static load of the ESL method is computed by using the transient displacements occurring peak and valley stresses. Therefore the time step size in the transient analysis affects the optimization results. In Fig. 16, the less material was used as the larger time interval was used for tran-

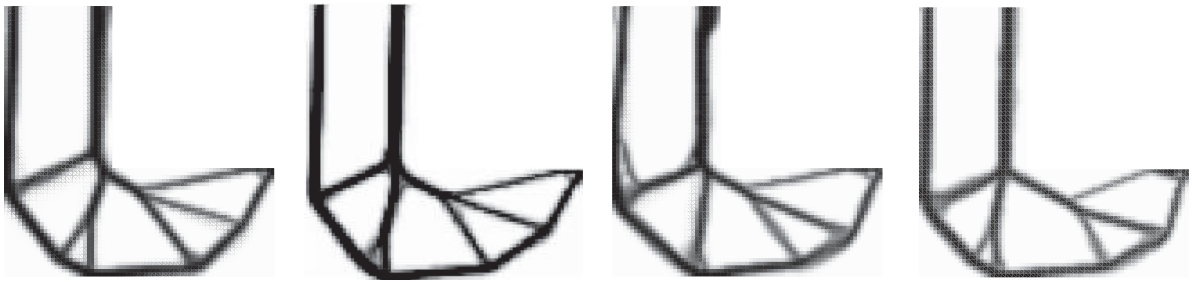

Fig. 16. Optimized shapes when the time step size are set to (a) 0.25 s ($V/V_0 = 0.278$, $D_{max} = 1.00$), (b) 0.5 s ($V/V_0 = 0.277$, $D_{max} = 1.02$), (c) 1.0 s ($V/V_0 = 0.264$, $D_{max} = 0.94$), and (d)1.5 s ($V/V_0 = 0.273$, $D_{max} = 0.94$).

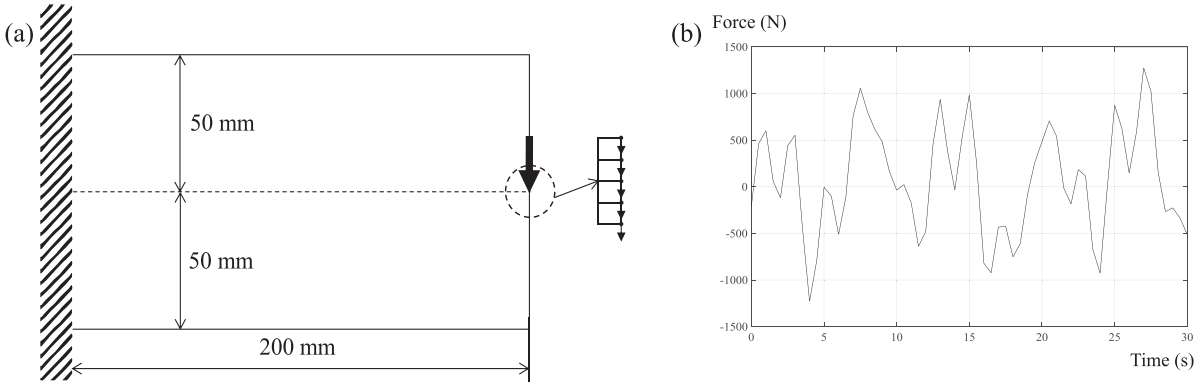

Fig. 17. A cantilever beam: (a) Design domain, boundary condition, applied loading position, and (b) the history of the mechanical force.

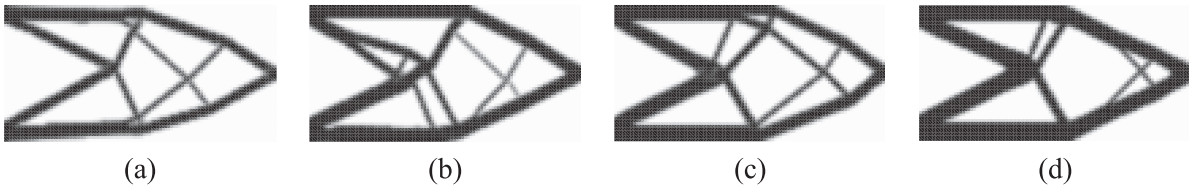

Fig. 18. Optimization results with respect to the scale factor: (a) scale factor = 8 ($V/V_0 = 0.294$, $D_{max} = 1.01$), (b) scale factor = 10 ($V/V_0 = 0.387$, $D_{max} = 0.99$), (c) scale factor = 12 ($V/V_0 = 0.426$, $D_{max} = 1.00$) and (d) scale factor = 14 ($V/V_0 = 0.425$, $D_{max} = 1.00$).

sient analysis. Because the peak and valley values of the time stress history become smaller according to the larger time step size, less material is used. Therefore, the present TO method requires accurate transient analysis.

4.3. Example 3: Cantilever beam

For the last example, a cantilever beam structure is considered. The design domain, the clamped boundary condition, and the applied variable amplitude loading positions are shown in Fig. 17. The design domain is discretized by the 5000 2-mm by 2-mm quadrilateral Q4 plane stress elements. The thickness of an element is set to 1 mm. The number of regions for p-norm calculation is set to 1. The value of p for the p-norm calculation is set to 4. Young's modulus, Poisson's ratio, and density are set to 210 GPa, 0.3, and 7820 kg/m^3, respectively. Also the desired minimum value for life is set to 10^6. To calculate the fatigue damage, the ultimate tensile strength in (18), S_{ut}, the fatigue damage strength coefficient, σ_f, and the exponent of the Basquin equation, b_f, in (17) are set to 380 MPa, 650 MPa, and −0.075, respectively. An optimization process finishes if the value of maximum change in the design variable between two sequential optimization iterations is smaller than 0.001 or the iteration number is larger than the maximum iteration number, 1000. Since the time required for one iteration of optimization is 17.6 s, it takes 17,600 s to complete the 1000 iterations.

In this example, we also investigate the effect of the scale factor. To find the best value for the scale factor, several values are considered and the results are plotted in Fig. 18.

This example shows that the scale factor largely affects the optimized result and convergence. With the scale factor larger than 8, the stable convergences can be obtained in Fig. 18(a). Some results with the larger scale factors are shown in Fig. 18 (b, c and d). The results with the scale factors larger than 10 are similar to the result of the compliance minimization

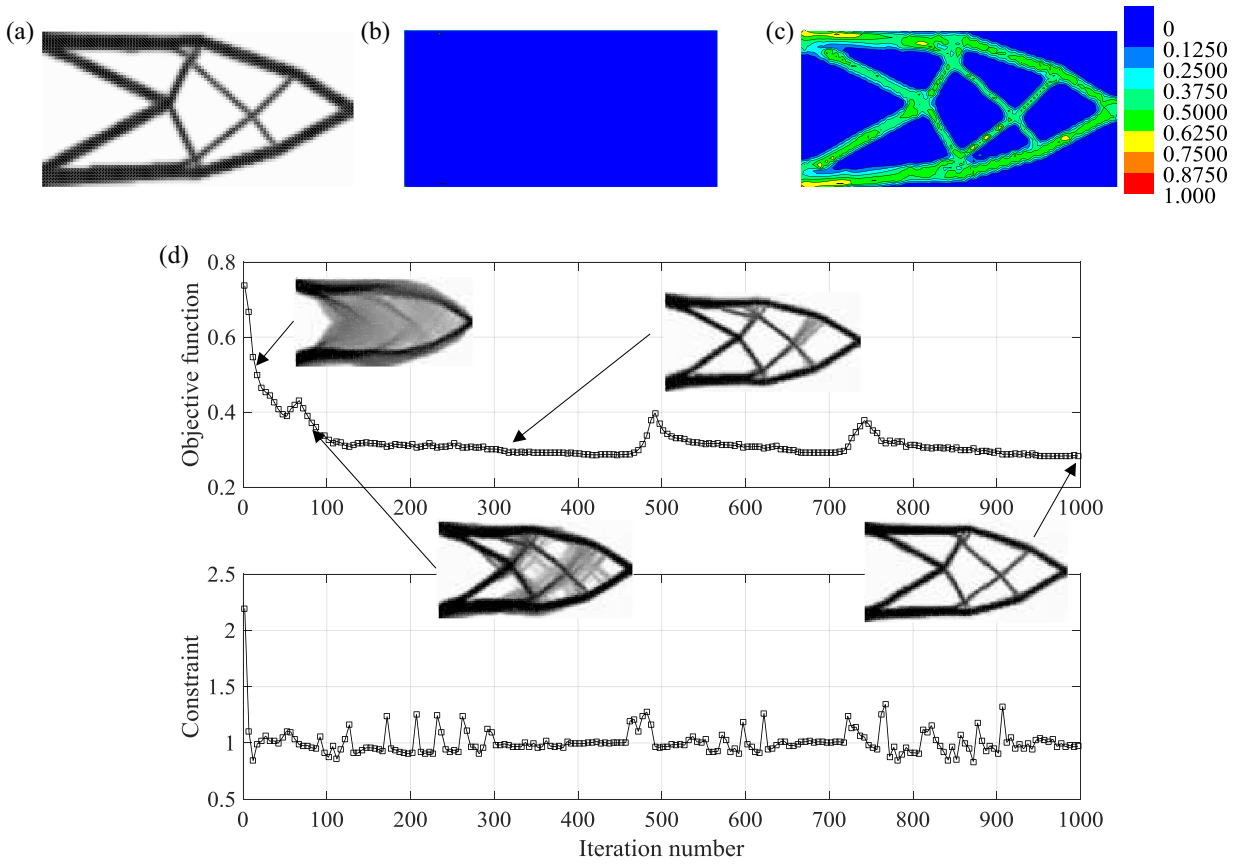

Fig. 19. Optimized shape and the damage distribution of the result using the scaled damage (scale factor = 8): (a) the optimized shape ($V/V_0 = 0.294$), (b) the distribution of the un-scaled damage ($D_{max} = 1.01$), (c) the distribution of the scaled damage ($\tilde{D}_{\max} = 1.00$), (d) the history of the objective function and the constraint.

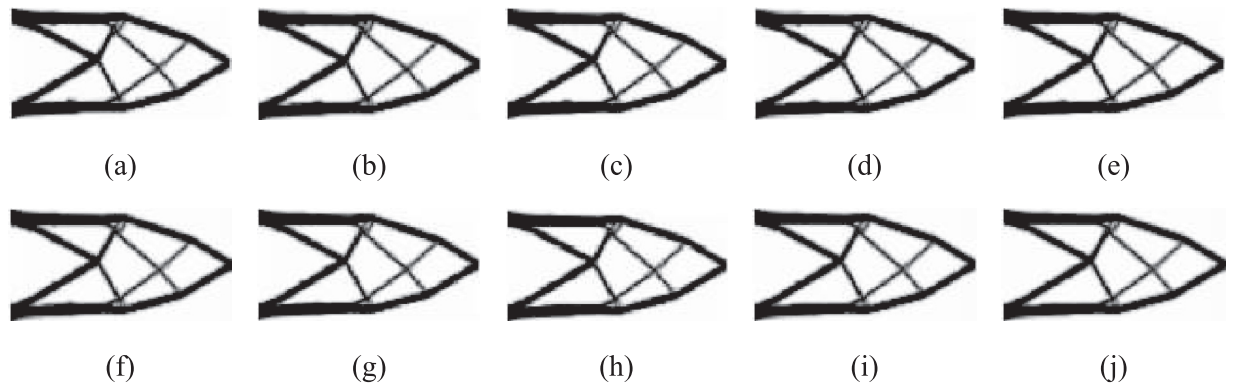

Fig. 20. Optimization history of layout in Fig. 19 at last 100 iterations with 10 intervals. Layouts obtained at (a) 910th, (b) 920th, (c) 930th, (d) 940th, (e) 950th, (f) 960th, (g) 970th, (h) 980th, (i) 990th, and (j) 1000th iteration.

problem. Through Example 2 and Example 3 our conclusion is that a scale factor between 8 and 10 which is smaller than $(-1/b_f)$ might give stable convergence. In Fig. 19 we represent the convergence history of cantilever beam example using a scale factor 8. The optimization finishes because the number of iteration reaches to the maximum number of iteration. As shown in Fig. 20, the obtained layouts at last 100 iterations do not change significantly but the maximum change of design variable between two sequential optimization iterations is larger than the specified value, 0.001, due to local optimum issue of stress or fatigue constrained topology optimization.

5. Conclusions

As fatigue is an important property for structural design to avoid catastrophic disaster, a new TO method is developed in this research to prevent fatigue occurring due to variable amplitude and proportional load based on the pseudo sensitivity analysis using the ESL approach. To estimate the cumulative fatigue damage, the transient time stress history is calculated by the Newmark method and the effective cycle is extracted by using the multiaxial cycle counting method of Wang and Brown.

The usefulness of the employed pseudo sensitivity analysis is verified by solving several optimization problems including a simple two-bar size optimization example. Comparing the sensitivities from FDM and the pseudo sensitivity analysis in the two-bar size optimization problem, it is observed that the difference of sensitivities between them converges during a design optimization process. It is also found that the result satisfied the stationary KKT condition. The scaling factor of the fatigue damage constraint is necessary because of the high sensitivity values to damage behavior depending on the changes of the stress magnitude. As the x-axis of S–N curve is based on a log scale, the fatigue damage concentration is more severe than the stress concentration. Therefore, it is very difficult to perform TO by using a pure damage constraint with the gradient based optimizer. Because the scaling approach relaxes the fatigue damage concentration in the design domain, we can obtain a TO result with stable convergence. By comparing the two-bar size and topology optimization, the validity and limitation of the present method was observed. The present TO gives an initial layout that is stable, but the result tends to be more localized compared with the size optimization result. A local optimum can be obtained in TO because of the p-norm constraint. The validity of the present TO method is verified by solving two kinds of TO problems. Because of the differences of compressive and tensile stresses on fatigue, an asymmetric layout can be obtained although the design domain and the boundary conditions are symmetric.

In summary, this research proposes a new TO method considering that the fatigue damage constraint occurs due to variable amplitude and proportional load. The pseudo sensitivity analysis approach using ESL for the transient system and the scaling of damage constraint is proposed. The validity of the present method is verified by solving some 2D problems.

Acknowledgement

This research was supported by the Fusion Research Program for Green Technologies through the National Research Foundation of Korea(NRF) funded by the Ministry of Science, ICT & Future Planning (No. NRF-2015R1A2A2A11027580)

References

[1] D.L. Logan, A First Course in the Finite Element Method, Cengage Learning, 2011.
[2] Y.-L. Lee, M.E. Barkey, H.-T. Kang, Metal Fatigue Analysis Handbook: Practical Problem-Solving Techniques For Computer-Aided Engineering, Elsevier, 2011.
[3] C. Wang, M. Brown, Life prediction techniques for variable amplitude multiaxial fatigue—part 2: comparison with experimental results, J. Eng. Mater. Technol. 118 (1996) 371–374.
[4] K. Suzuki, N. Kikuchi, A homogenization method for shape and topology optimization, Comput. Methods Appl. Mech. Eng. 93 (1991) 291–318.
[5] J.D. Deaton, R.V. Grandhi, A survey of structural and multidisciplinary continuum topology optimization: post 2000, Struct. Multidiscip. Optim. 49 (2014) 1–38.
[6] X. Duan, X. Qin, F. Li, Topology optimization of Stokes flow using an implicit coupled level set method, Appl. Math. Model. 40 (2016) 5431–5441.
[7] A. Molter, J.S.O. Fonseca, L. dos Santos Fernandez, Simultaneous topology optimization of structure and piezoelectric actuators distribution, Appl. Math. Model. 40 (2016) 5576–5588.
[8] W.J.P. Casas, R. Pavanello, Optimization of fluid-structure systems by eigenvalues gap separation with sensitivity analysis, Appl. Math. Model. 42 (2017) 269–289.
[9] M.P. Bendsøe, O. Sigmund, Material interpolation schemes in topology optimization, Arch. Appl. Mech. 69 (1999) 635–654.
[10] M.P. Bendsoe, O. Sigmund, Topology Optimization: Theory, Methods and Applications, Springer Science & Business Media, 2003.
[11] J.-H. Zhu, W.-H. Zhang, L. Xia, Topology optimization in aircraft and aerospace structures design, Arch. Comput. Methods Eng. 23 (2016) 595–622.
[12] O. Sigmund, On the design of compliant mechanisms using topology optimization, J. Struct. Mech. 25 (1997) 493–524.
[13] S. Nishiwaki, M.I. Frecker, S. Min, N. Kikuchi, Topology optimization of compliant mechanisms using the homogenization method, (1998).
[14] M. Frecker, N. Kikuchi, S. Kota, Topology optimization of compliant mechanisms with multiple outputs, Struct. Multidiscip. Optim. 17 (1999) 269–278.
[15] T.E. Bruns, D.A. Tortorelli, Topology optimization of non-linear elastic structures and compliant mechanisms, Comput. Methods Appl. Mech. Eng. 190 (2001) 3443–3459.
[16] A.R. Díaaz, N. Kikuchi, Solutions to shape and topology eigenvalue optimization problems using a homogenization method, Int. J. Numer. Methods Eng. 35 (1992) 1487–1502.
[17] I. Hagiwara, Eigen frequency maximization of plates by optimization of topology using homogenization and mathematical programming, JSME Int. J. Ser. C, Dyn. Control, Rob. Des. Manuf. 37 (1994) 667–677.
[18] Z.-D. Ma, N. Kikuchi, H.-C. Cheng, Topological design for vibrating structures, Comput. Methods Appl. Mech. Eng. 121 (1995) 259–280.
[19] N.L. Pedersen, Maximization of eigenvalues using topology optimization, Struct. Multidiscip. Optim. 20 (2000) 2–11.
[20] C. Jog, Topology design of structures subjected to periodic loading, J. Sound Vib. 253 (2002) 687–709.
[21] M. Bruggi, P. Venini, Eigenvalue-based optimization of incompressible media using mixed finite elements with application to isolation devices, Comput. Methods Appl. Mech. Eng. 197 (2008) 1262–1279.
[22] G.H. Yoon, Maximizing the fundamental Eigen frequency of geometrically nonlinear structures by topology optimization based on element connectivity parameterization, Comput. Struct. 88 (2010) 120–133.
[23] R. Yang, C. Chen, Stress-based topology optimization, Struct. Optim. 12 (1996) 98–105.
[24] M. Bruggi, On an alternative approach to stress constraints relaxation in topology optimization, Struct. Multidiscip. Optim. 36 (2008) 125–141.
[25] C. Le, J. Norato, T. Bruns, C. Ha, D. Tortorelli, Stress-based topology optimization for continua, Struct. Multidiscip. Optim. 41 (2010) 605–620.
[26] S.H. Jeong, S.H. Park, D.-H. Choi, G.H. Yoon, Topology optimization considering static failure theories for ductile and brittle materials, Comput. Struct. 110 (2012) 116–132.
[27] Y. Luo, Z. Kang, Topology optimization of continuum structures with Drucker–Prager yield stress constraints, Comput. Struct. 90 (2012) 65–75.

[28] H. Liu, W. Zhang, T. Gao, A comparative study of dynamic analysis methods for structural topology optimization under harmonic force excitations, Struct. Multidiscip. Optim. 51 (2015) 1321–1333.
[29] W. Zhang, H. Liu, T. Gao, Topology optimization of large-scale structures subjected to stationary random excitation: an efficient optimization procedure integrating pseudo excitation method and mode acceleration method, Comput. Struct. 158 (2015) 61–70.
[30] R. Ghelichi, A. Bernasconi, M. Guagliano, Geometrical optimization of notches under multi-axial fatigue loading, Int. J. Fatigue 33 (2011) 985–991.
[31] N. Govindarajan, Multi axial high cycle fatigue life model optimization for drilling tools, Pet. Explor. Dev. 42 (2015) 884–887.
[32] J. Oest, E. Lund, Topology optimization with finite-life fatigue constraints, Struct. Multidiscip. Optim. 56 (2017) 1–15.
[33] E. Holmberg, B. Torstenfelt, A. Klarbring, Fatigue constrained topology optimization, Struct. Multidiscip. Optim. 50 (2014) 207–219.
[34] K. Sherif, W. Witteveen, K. Puchner, H. Irschik, Efficient topology optimization of large dynamic finite element systems using fatigue, AIAA J. 48 (2010) 1339.
[35] M.W. Mrzygłód, M. Kurek, T. Łagoda, The application of the criteria of multiaxial fatigue in the critical plane for the topology optimization of a structure, in: AIP Conference Proceedings, AIP Publishing, 2016.
[36] M. Mrzygłód, Two-stage optimization method with fatigue constraints for thin-walled structures, J. Theor. Appl. Mech. 48 (2010) 567–578.
[37] P. Duysinx, M. Collet, S. Bauduin, E. Tromme, L. Noel, M. Bruggi, Topology optimization of mechanical and aerospace components subject to fatigue stress constraints, (2015).
[38] J.W. Lee, G.H. Yoon, S.H. Jeong, Topology optimization considering fatigue life in the frequency domain, Comput. Math. Appl. 70 (2015) 1852–1877.
[39] E. Pagnacco, S. Lambert, L. Khalij, D. Rade, Design optimisation of linear structures subjected to dynamic random loads with respect to fatigue life, Int. J. Fatigue 43 (2012) 168–177.
[40] S.H. Jeong, D.-H. Choi, G.H. Yoon, Fatigue and static failure considerations using a topology optimization method, Appl. Math. Model. 39 (2015) 1137–1162.
[41] W. Choi, G. Park, Transformation of dynamic loads into equivalent static loads based on modal analysis, Int. J. Numer. Methods Eng. 46 (1999) 29–43.
[42] B. Kang, W. Choi, G. Park, Structural optimization under equivalent static loads transformed from dynamic loads based on displacement, Comput. Struct. 79 (2001) 145–154.
[43] G. Park, B. Kang, Validation of a structural optimization algorithm transforming dynamic loads into equivalent static loads, J. Optim. Theory Appl. 118 (2003) 191–200.
[44] Y. Kim, G. Park, R. Kolonay, M. Blair, R. Canfield, Nonlinear dynamic response structural optimization of a joined-wing using equivalent static loads, J. Aircraft 46 (2009) 821.
[45] Y.-I. Kim, G.-J. Park, Nonlinear dynamic response structural optimization using equivalent static loads, Comput. Methods Appl. Mech. Eng. 199 (2010) 660–676.
[46] S.J. Moon, G.H. Yoon, A newly developed qp-relaxation method for element connectivity parameterization to achieve stress-based topology optimization for geometrically nonlinear structures, Comput. Methods Appl. Mech. Eng. 265 (2013) 226–241.
[47] J. París, F. Navarrina, I. Colominas, M. Casteleiro, Improvements in the treatment of stress constraints in structural topology optimization problems, J. Comput. Appl. Math. 234 (2010) 2231–2238.
[48] G. Qiu, X. Li, A note on the derivation of global stress constraints, Struct. Multidiscip. Optim. 40 (2010) 625.
[49] J.E. Shigley, Shigley's Mechanical Engineering Design, Tata McGraw-Hill Education, 2011.
[50] K. Svanberg, The method of moving asymptotes—a new method for structural optimization, Int. J. Numer. Methods Eng. 24 (1987) 359–373.
[51] C. Fleury, CONLIN: an efficient dual optimizer based on convex approximation concepts, Struct. Optim. 1 (1989) 81–89.
[52] J. París, F. Navarrina, I. Colominas, M. Casteleiro, Topology optimization of continuum structures with local and global stress constraints, Struct. Multidiscip. Optim. 39 (2009) 419–437.
[53] J. París, F. Navarrina, I. Colominas, M. Casteleiro, Block aggregation of stress constraints in topology optimization of structures, Adv. Eng. Softw. 41 (2010) 433–441.